Pattern formation in the one-dimensional Gray-Scott model

Doelman, A.; Kaper, T.J.; Zegeling, P.A.

DOI
10.1088/0951-7715/10/2/013
Publication date
1997

Published in
Nonlinearity

Nonlinearity **10** (1997) 523–563. Printed in the UK PII: S0951-7715(97)77566-2

Pattern formation in the one-dimensional Gray–Scott model

Arjen Doelman†, Tasso J Kaper‡ and Paul A Zegeling†

† Mathematisch Instituut, Universiteit Utrecht, PO Box 80.010, 3508TA Utrecht, The Netherlands

‡ Department of Mathematics, Boston University, Boston, MA 02215, USA

Received 18 April 1996, in final form 3 September 1996
Recommended by E Knobloch

Abstract. In this work, we analyse a pair of one-dimensional coupled reaction-diffusion equations known as the Gray–Scott model, in which self-replicating patterns have been observed. We focus on stationary and travelling patterns, and begin by deriving the asymptotic scaling of the parameters and variables necessary for the analysis of these patterns. Single-pulse and multi-pulse stationary waves are shown to exist in the appropriately scaled equations on the infinite line. A (single) pulse is a narrow interval in which the concentration U of one chemical is small, while that of the second, V, is large, and outside of which the concentration U tends (slowly) to the homogeneous steady state $U \equiv 1$, while V is everywhere close to $V \equiv 0$. In addition, we establish the existence of a plethora of periodic steady states consisting of periodic arrays of pulses interspersed by intervals in which the concentration V is exponentially small and U varies slowly. These periodic states are spatially inhomogeneous steady patterns whose length scales are determined exclusively by the reactions of the chemicals and their diffusions, and not by other mechanisms such as boundary conditions. A complete bifurcation study of these solutions is presented. We also establish the non-existence of travelling solitary pulses in this system. This non-existence result reflects the system's degeneracy and indicates that some event, for example pulse splitting, 'must' occur when two pulses move apart from each other (as has been observed in simulations): these pulses evolve towards the non-existent travelling solitary pulses. The main mathematical techniques employed in this analysis of the stationary and travelling patterns are geometric singular perturbation theory and adiabatic Melnikov theory.

Finally, the theoretical results are compared to those obtained from direct numerical simulation of the coupled partial differential equations on a 'very large' domain, using a moving grid code. It has been checked that the boundaries do not influence the dynamics. A subset of the family of stationary single pulses appears to be stable. This subset determines the boundary of a region in parameter space in which the self-replicating process takes place. In that region, we observe that the core of a time-dependent self-replicating pattern turns out to be precisely a stationary periodic pulse pattern of the type that we construct. Moreover, the simulations reveal some other essential components of the pulse-splitting process and provide an important guide to further analysis.

AMS classification scheme numbers: 35K57, 34C37, 35B10, 35B32, 35Q80, 34E15, 65M06, 34C30

1. Introduction

Self-replicating patterns have recently been observed in a reaction-diffusion system [21, 17, 22]. Numerical simulations show that the irreversible Gray–Scott model exhibits a broad array of new patterns, including spots that self replicate in a self-sustaining fashion

and develop into a variety of time-dependent and time-independent asymptotic states in two dimensions [21], as well as pulses that self replicate in one dimension [22]. The two-dimensional self-replicating spots have also been observed experimentally in a ferrocyanide–iodate–sulfite reaction [17]. See [16] for more details of the set-up. Moreover, those same experiments led to the discovery of other new patterns, such as annular patterns emerging from circular spots [17].

The irreversible Gray–Scott model governs the chemical reactions $\mathcal{U} + 2\mathcal{V} \to 3\mathcal{V}$ and $\mathcal{V} \to \mathcal{P}$ in a gel reactor, where $\mathcal{V}$ catalyses its own reaction with $\mathcal{U}$ and $\mathcal{P}$ is an inert product (see [9–11]). The gel reactor is coupled to a reservoir in which the concentrations of $\mathcal{U}$ and $\mathcal{V}$ are maintained constant. This coupling also results in both chemicals being removed from the reactor in a concentration-dependent fashion. Furthermore, the diffusivities, D_U and D_V, of the chemicals $\mathcal{U}$ and $\mathcal{V}$, respectively, can be any chemically relevant positive numbers. For example, in the one-dimensional work [22], pulse splitting was observed when $D_U = 1$ and $D_V = \delta^2 = 0.01$. By contrast, in the two-dimensional numerical simulations [21], the spot replication was observed with $D_U = 2D_V = 2 \times 10^{-5}$, and other studies have focused on the case of equal or nearly equal diffusivities, see for example [20, 25, 30].

Letting $U = U(x, t)$ and $V = V(x, t)$ denote the concentrations of the two chemical species $\mathcal{U}$ and $\mathcal{V}$, the pair of coupled reaction-diffusion equations governing these reactions is:

$$\begin{aligned} \frac{\partial U}{\partial t} &= D_U \nabla^2 U - UV^2 + A(1 - U) \\ \frac{\partial V}{\partial t} &= D_V \nabla^2 V + UV^2 - BV. \end{aligned}$$

Here, A denotes the rate at which $\mathcal{U}$ is fed from the reservoir into the reactor (and this same feed process takes $\mathcal{U}$ and $\mathcal{V}$ out in a concentration-dependent way), the concentration of $\mathcal{V}$ in the reservoir is assumed to be zero, and B is the sum of A and the rate constant k_2, which equals the rate at which $\mathcal{V}$ is converted to an inert product.

A pulse in one space dimension (and similarly a spot in two space dimensions) may loosely be defined as an interval (region) of high V and low U. Outside of such an interval (region) U is near one and V is near zero. A pulse widens (a spot grows) when the flux of $\mathcal{U}$ into it is high enough to sustain the first reaction and replenish the amount of the chemical $\mathcal{V}$ that leaves the pulse (spot) through diffusion and the coupling to the reservoir. Moreover, as a pulse widens (or a spot grows), the middle can quickly cave in (the spot gets pinched into two) when insufficient amounts of $\mathcal{U}$ reach the middle to sustain a high V. Thus, a pulse (spot) can undergo a division process, and the two pulses (spots) can move away from each other using up the $\mathcal{U}$ from adjacent intervals (regions). This initial splitting is stationary in the sense that the centre of the pattern stays at the middle of the domain. Further, dynamic pulse splitting occurs when there is enough $\mathcal{U}$ behind the moving pulse, and a new pulse emerges on the trailing edge.

In order to study this rich pulse dynamics mathematically, we analyse the irreversible Gray–Scott model in one space dimension ($x \in \mathbb{R}$ and $\nabla^2 = \partial^2/\partial x^2$) on the infinite line:

$$\begin{aligned} \frac{\partial U}{\partial t} &= \nabla^2 U - UV^2 + A(1 - U) \\ \frac{\partial V}{\partial t} &= \delta^2 \nabla^2 V + UV^2 - BV \end{aligned} \tag{1.1}$$

where $0 < \delta^2 \ll 1$. The choice of $D_U = 1$ and $D_V = \delta^2 \ll 1$ here follows that of [22], where it is explained that this singular limit 'clarifies which physical processes are dominant as the system evolves'.

The numerical simulations of [22] and of this work (see section 6) suggest that neither U nor V are $\mathcal{O}(1)$ throughout the whole pattern. For instance, during a peak in V, it is observed that V is 'large' ($\gg 1$), while U becomes 'small' ($\ll 1$). Therefore, we first perform a detailed scaling analysis that results in a scaled system in which the variables and parameters are $\mathcal{O}(1)$. Based on geometrical arguments, these scalings enable us to deduce that A must be $\mathcal{O}(\delta^2)$ in (1.1) in order for the patterns we find to exist. They also lead us to the correct asymptotic scalings for the variables and the other parameter B.

Our main results are then the following. First, we prove the existence of single-pulse and multi-pulse stationary states for (1.1) on the infinite line. The detailed asymptotic scalings are derived specifically for this result, and are shown to be essential. As remarked above, A must scale with the small parameter δ^2 in order for these pulses to exist. Moreover, we show that the relevant scalings for a pulse are $U = \mathcal{O}(\delta^{\alpha})$, $V = \mathcal{O}(\delta^{-\alpha/3})$, and $B = \mathcal{O}(\delta^{2\alpha/3})$, where $\alpha \in [0, \frac{3}{2})$. In between the pulses of a multi-pulse solution, V becomes $\ll 1$ but not too small; whereas, in the semi-infinite intervals surrounding the pulses, V becomes exponentially small. Also, we are able to construct these solutions for each (rescaled) A and B and $\alpha \in [0, \frac{3}{2})$.

Second, we establish the existence of a plethora of periodic stationary states for (1.1) on the infinite line (equivalently for (1.1) on a finite interval with periodic boundary conditions). These periodic states consist of a infinite array of narrow, equally spaced pulses. The same scalings derived for the above stationary multi-pulse states are also central to the analysis here. During a pulse event, the dependent variables U and V scale exactly as in the above multi-pulse states. Here, however, V is exponentially small in the intervals between pulses. Most importantly, these periodic states are observed to form the core regions of the time-dependent self-replicating pulse patterns on finite domains, and it is found that their intrinsic length scale is determined exclusively by the reaction and diffusion of the chemicals, and not by boundary effects.

Third, the travelling pulses observed in the simulations of [22] and of this work are, for large time intervals, more or less stationary in a co-moving frame. Hence, it is natural to try to construct travelling pulses of the same type as the stationary pulses. However, we prove that these travelling solutions cannot exist. Therefore, this non-existence result shows that, while the numerically observed moving pulses begin to resemble the non-existing travelling solitary pulses more and more, they must undergo some transformation, such as pulse splitting. Moreover, we note that the analysis needed to obtain this result, while again depending on the above scaling, is delicate, since the non-existence of travelling waves violates simple generic counting arguments (see section 5).

Finally, we present the results of some numerical simulations of (1.1) on finite, but sufficiently large, domains with various types of boundary conditions, using a moving grid code. These simulation results corroborate our analytical results and confirm that the patterns do not form in response to boundary conditions. In the (rescaled) (A, B)-parameter plane we determine a transition region which distinguishes two regions: a trivial one where (U, V) tend to the asymptotically stable homogeneous 'pattern' $U \equiv 1$, $V \equiv 0$, and the so-called self-replicating pulse region. In this transition region we observe the stationary single-pulse patterns described above. Above the transition region, namely in the self-replicating pulse region, one does not expect, *a priori*, stationary behaviour. Nevertheless, we observe that (after quite a long time) the self-replicating patterns on an unbounded domain evolve towards a stationary periodic pulse pattern that grows at both sides by a self-replication process which only involves the two travelling 'boundary pulses' and their most recently created 'images'. The periodic 'core' is once again of the type described above. We have made a quantitative check between the observed patterns and those we

constructed analytically and found a very good agreement. Note that the periodic core itself turns out to be the asymptotically stable pattern if one considers a finite domain with periodic boundary conditions (see figure 1 in [22]). Moreover, the simulations reveal some other essential components of the pulse-splitting process and provide an important guide to further analysis. In the discussion we suggest some ideas for future work.

Our analysis begins with the travelling wave ansatz: $U = u(x-ct)$ and $V = v(x-ct)$, where $c \in \mathbb{R}$ is the wave speed, and $c = 0$ corresponds to stationary states. Plugging this ansatz into (1.1) yields the following system of four ordinary differential equations:

$$\begin{aligned} u' &= p \\ p' &= -cp + uv^2 - A(1-u) \\ \delta v' &= q \\ \delta q' &= -\frac{c}{\delta} q - uv^2 + Bv \end{aligned} \tag{1.2}$$

where $'$ denotes the derivative with respect to the independent variable $\xi \equiv x - ct$. Note that the fourth component of the vector field (1.2) is $\mathcal{O}(\frac{1}{\delta})$ if $c = \mathcal{O}(1)$, therefore we introduce γ by

$$c = \delta\gamma. \tag{1.3}$$

Rescaling the independent variable $\xi \equiv \delta\eta$ yields:

$$\begin{aligned} \dot{u} &= \delta p \\ \dot{p} &= \delta[-\delta\gamma p + uv^2 - A(1-u)] \\ \dot{v} &= q \\ \dot{q} &= -\gamma q - uv^2 + Bv \end{aligned} \tag{1.4}$$

where $\dot{}$ denotes the derivative with respect to the new independent variable η.

Equation (1.4) possesses two time scales: u and p are slow variables, and v and q are fast variables. Hence, the system (1.4) splits into reduced slow and fast subsystems in a natural fashion. The reduced slow subsystem is defined only on the invariant plane $\{u, p, v = 0, q = 0\} \stackrel{\text{def}}{=} \mathcal{M}$ and is given by $u'' + \delta\gamma u' + A(1-u) = 0$, which has an equilibrium at $(u = 1, u' = 0)$. The reduced fast subsystem is the nonlinear planar oscillator $\ddot{v} + \gamma\dot{v} + uv^2 - Bv = 0$, where the variable, u, is treated as a fixed parameter, and where this oscillator possesses an orbit homoclinic to $(v = 0, \dot{v} = q = 0)$ when $\gamma = 0$ (equivalently $c = 0$).

This analytical splitting has a natural geometric analogue that manifests itself in the various types of observed pulse solutions and that will be exploited throughout this work. Indeed, based on the structure of the pulse solutions observed in our numerical simulations and those reported in figures 1 and 2 of [22, 3], respectively, we construct solutions which consist of alternating distinguished slow ($= \mathcal{O}(\delta)$) and fast ($= \mathcal{O}(1)$) parts. The slow part of the solution is guided by a particular slow trajectory on the invariant plane, or slow manifold, $\mathcal{M} = \{u, p, v = 0, q = 0\}$, while $|v|, |q| \ll 1$ in (1.4). By contrast, the fast part of the solution is guided by a particular homoclinic orbit of the reduced fast system, since u and p will change by an $\mathcal{O}(\delta)$ amount during a fast excursion through (v, q) space.

More precisely, we employ adiabatic Melnikov theory [19, 24, 32] directly on the scaled version of (1.4) to determine where the stable and unstable manifolds of the invariant slow plane intersect. This theory is particularly simple when $c = 0$, since (the scaled version of) (1.4) has a nice symmetry then. The case $c > 0$ is much more involved, however, and it is necessary to calculate the asymptotic expansions for the location of the intersection out

to a fairly high order. Furthermore, for both cases $c = 0$ and $c > 0$, it is also necessary to calculate the asymptotic expansions for the base points of the fast stable and unstable fibres lying in the transverse intersection of the slow plane's stable and unstable manifolds; again to sufficiently high order when $c > 0$. In this respect, we make use of the fundamental work [7] in geometric singular perturbation theory to study how the fast and slow dynamics 'hook up' to each other.

By constructing fast–slow periodic and homoclinic solutions of the type just described to a version of (1.4) in which the variables and parameters are properly scaled, we obtain our first and second main results. In particular, the locally unique homoclinic orbits of (1.4) that we find—which are biasymptotic to the equilibrium point $(u = 1, u' = 0)$ of the slow subsystem and which are comprised of one or more fast excursions into in the $v - q$ space—immediately imply the existence of single-pulse and multi-pulse stationary states of (1.1) on the infinite line. In addition, each of the periodic orbits of (1.4)—consisting of slow segments near $\mathcal{M}$ and fast excursions away from $\mathcal{M}$ into the $v - q$ space—whose existence we prove is precisely a periodic stationary state of (1.1). These $c = 0$ periodic orbits are locally unique and lie exponentially close to the transverse intersections found above using adiabatic Melnikov theory, by a modified version [27] of the exchange lemma with exponentially small error [13]. Finally, the dynamics of (1.4) also holds the key to our proof of the non-existence of travelling waves.

The periodic patterns we observe are Turing patterns because they are found to have an intrinsic chemical wavelength as described above. However, they are not formed by the bifurcation mechanism Turing proposed [29], because they do not appear to emerge from small inhomogeneities in linearly unstable homogeneous steady states. Rather, the initial data taken for most of our simulations are localized, large-amplitude perturbations from the homogeneous steady state $(U = 1, V = 0)$, which is linearly stable for all positive values of the parameters A and B. See [14] for a recent review of Turing patterns and spiral waves in reaction-diffusion systems, and note that [31] show that D_U/D_V must exceed a critical ratio for supercritical bifurcations to occur.

The work here on the irreversible Gray–Scott model involving equations (1.1) fits into the larger problem area of the reversible Gray–Scott model, see for instance [11], equation (5) in [30], or equation (1) of [25]. The work reported in [30] shows that steady spatial patterns may form, for example, from finite-amplitude perturbations of a stable homogeneous steady state, when the diffusion coefficients of all three species are equal. Also, in [25], it is shown, under the same assumption of equal diffusivities, that the presence of external gradients leads to Hopf bifurcations from spatially homogeneous states to periodic states as well as transitions to other patterns, including multi-hump branches and fronts. In [6] and [8] patterns that develop from finite-amplitude perturbations to linearly stable homogeneous states are studied in one- and two-dimensional FitzHugh–Nagumo models. In one dimension, the existence of large-amplitude multi-pulse and periodic stationary waves is shown when the diffusivity of the inhibitor is large, see [6]. Note that one of the major differences between the FitzHugh–Nagumo and the Gray–Scott models is the existence of an excitation threshold in the former. Finally, we remark that multi-peak and periodic patterns have also recently been observed in models of the Belousov–Zhabotinsky reaction, see [1, 26], respectively.

Equations of the form (1.1) with $A, B = 0$ are also of interest. The recent work [18] investigates the dynamics of propagating fronts in this autocatalytic reaction. There, a new phenomenon, dubbed biscale chaos, that occurs under the same condition imposed here is reported and analysed, namely that the diffusivity of the 'fuel' $\mathcal{U}$ is sufficiently larger than the diffusivity of the 'autocatalyst' $\mathcal{V}$, although with qualitatively different initial data.

Finally, we remark that other localized phenomena are reported in [4] for a system of reaction-diffusion equations related to (1.1) but with a small parameter in front of the term $\partial V/\partial t$.

The paper is organized as follows. In section 2, we perform the scaling analysis that puts (1.4) into the form suitable for the analysis presented in the remainder of the paper. The global geometry of the rescaled system is studied in section 3, where we explicitly identify distinguished fast and slow orbit segments. In section 4, we use the results from section 3 to construct stationary single-pulse and multi-pulse homoclinic solutions as well as a plethora of periodic steady-state solutions. The non-existence of travelling waves is shown in section 5. The theoretical results of sections 4 and 5 are compared to those of numerical simulations in section 6. Finally, we discuss a variety of issues related to our results and suggest further work in section 7.

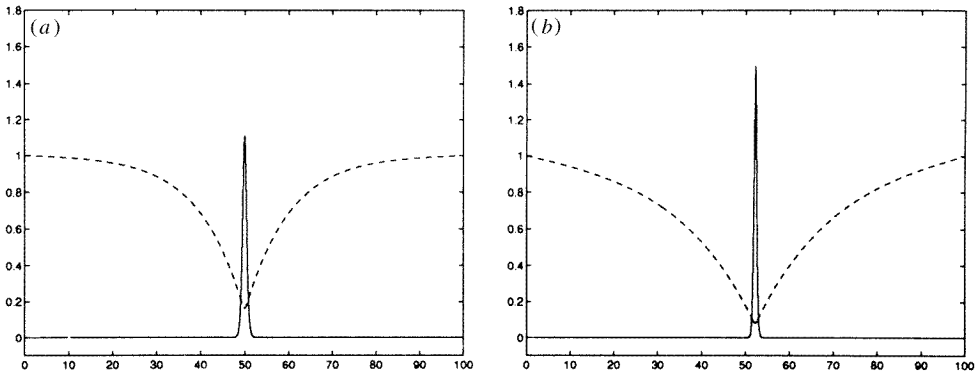

Figure 1. Stationary one-pulse homoclinic orbits observed in numerical simulations of (1.1) at time $t = 1000$: (a) $A = 0.01$, $B \approx 0.13$, $\delta^2 = 0.01$; (b) $A = 0.003$, $B \approx 0.086$, $\delta^2 = 0.003$. Note that by equation (2.4) and remark 2.2, $a = 1$ and $b = 0.6$ in both (a) and (b). The concentration U is given by a broken curve, and the concentration V is denoted by a full curve.

2. Scaling

A priori, it is not clear that it is necessary to introduce new scales in (1.4). However, we shall show in this section that the patterns observed in the numerical simulations correspond to solutions of (1.4) in which most quantities are not of $\mathcal{O}(1)$, at least not for all η. In figure 1, we present plots of two stable, stationary singular patterns which were obtained by numerical simulation of (1.1) for different choices of the parameters (δ, A, B); we refer to section 6 for a detailed description of the numerical analysis. In these simulations, the concentrations V and U are plotted as full and broken curves, respectively. V is almost everywhere small, except for one high 'peak,' while U is everywhere $\mathcal{O}(1)$, except in the peak region. To be more precise, in the peak region, the maximum of V scales as a negative power of δ and $0 < U \ll 1$, and outside of the peak regions, V is exponentially small in δ. Finally, the values of A and B are also not $\mathcal{O}(1)$: $A = 0.01 = \delta^2$, $B \approx 0.13$ in figure 1(a), $A = 0.003 = \delta^2$, $B \approx 0.086$ in figure 1(b). Therefore, in this section we shall present the relevant scalings of all quantities; their derivation is given in the appendix.

In the derivation of the appropriate scalings, we focus on the construction of solutions homoclinic to the saddle point $S = (1, 0, 0, 0)$ of (1.4). See figure 2(a) for a diagram of a one-pulse homoclinic orbit in phase space when $\gamma = 0$. Note that these homoclinic solutions

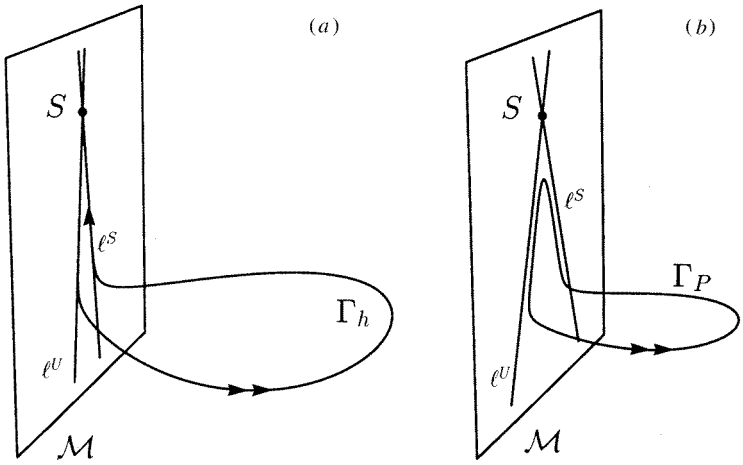

Figure 2. Schematic illustrations of (a) the one-pulse homoclinic orbit $\Gamma_h(t) \subset W^S(S) \cap W^U(S)$ and (b) a periodic orbit $\Gamma_P(t)$ in the four-dimensional phase space of (2.9) with, for simplicity, $\gamma = 0$. Note that these schematic illustrations show the slow segments in (p, u) coordinates and the fast segments in $(v, -q)$ coordinates.

correspond exactly to the stationary patterns shown in figure 1: $\lim_{|x|\to\infty} u(x,t) = 1$, $\lim_{|x|\to\infty} v(x,t) = 0$, $V \approx 0$ except for a 'fast' jump through the phase space. However, while the patterns shown in figure 1 are stationary, we perform the scaling analysis for the more general case of travelling waves in this section. Also, we remark that the restriction to homoclinic solutions is not essential in the derivation of the new scalings: the same scalings will be used in section 4.2 where we study periodic solutions, see figure 2(b).

First, we introduce a by

$$A = \delta^2 a. \tag{2.1}$$

This scaling of A agrees completely with the numerical values chosen for the simulations presented in figures 1(a) and (b): $A = \delta^2$ in both cases. Moreover, $A = 0.02$ while $\delta^2 = 0.01$ in the simulations in [22]. Analytically, the rationale for scaling A in this manner may be seen as follows. The saddle point, S, of (1.4) has two-dimensional stable and unstable manifolds, $W^S(S)$ and $W^U(S)$. The flow induced by (1.4) restricted to $\mathcal{M}$ is linear, therefore the intersections $W^S(S) \cap \mathcal{M}$ and $W^U(S) \cap \mathcal{M}$ are straight lines in $\mathcal{M}$ (see also figure 3 in which the diagram is for $\gamma = 0$, and see section 3.1):

$$\ell^{U,S} \equiv \left\{ p = \tfrac{1}{2}\left(\pm\sqrt{4A + \delta^2\gamma^2} - \delta\gamma \right)(u-1) \right\} \tag{2.2}$$

where $\ell^U \subset W^U(S)$ corresponds with the $+$ sign and $\ell^S \subset W^S(S)$ with the $-$ sign. The desired homoclinic solution $\Gamma_h(\eta) \subset W^S(S) \cap W^U(S)$ consists of three parts: first a slow part close to ℓ^U, then there is a fast excursion followed by the third part close to ℓ^S, which is again slow, see figure 2(a). The fast excursion 'jumps' from ℓ^U to ℓ^S; and hence, ℓ^U and ℓ^S need to be $\mathcal{O}(\delta)$ close to each other at the 'take-off' and 'touch-down' points of the fast excursion. It follows from (2.2) that the jump must occur $\mathcal{O}(\delta)$ near S (and thus $1 - u = \mathcal{O}(\delta)$). However, the numerically observed patterns show that u is not close to 1 during the excursion. By (2.2), we observe that an $\mathcal{O}(\delta)$ jump from ℓ^U to ℓ^S through the fast field for $1 - u \neq \mathcal{O}(\delta)$ is only possible if $A = \mathcal{O}(\delta^2)$: then ℓ^U and ℓ^S are $\mathcal{O}(\delta)$ close for all u of $\mathcal{O}(1)$. Hence, we arrive at (2.1).

Next, figures 1(*a*) and (*b*) indicate that $u \neq \mathcal{O}(1)$ during the excursion through the fast field (see also section 6). Also, it is clear from the fast subsystem of (1.4) that γ cannot be $\mathcal{O}(1)$: a solution which leaves the slow manifold $\mathcal{M}$ will follow the unstable manifold of the point $(0, 0)$ of this subsystem $\mathcal{O}(\delta)$ close. This orbit cannot return $\mathcal{O}(\delta)$ close to $\mathcal{M}$, due to the strong 'friction' term $-\gamma q$. Thus, we scale:

$$u = \delta^{\alpha}\hat{u} \qquad \text{and} \qquad \gamma = \delta^{\beta}\hat{\gamma} \tag{2.3}$$

where $\alpha \geqslant 0$ and $\beta > 0$ are, so far, free parameters. This scaling assumes that $\hat{u}$ cannot be smaller than $\mathcal{O}(1)$ during the excursion through the fast field: $\delta^{\alpha}\hat{u}$ is the leading order part of u during a 'jump'. Similarly, either $\hat{\gamma} = 0$, which corresponds to stationary waves, or $\hat{\gamma}$ is $\mathcal{O}(1)$, and not smaller. These properties of $\hat{u}$ and $\hat{\gamma}$ will be essential in the proof of the non-existence result of section 5.

Based on the above 'ansatz' (2.3), one has to rescale η, p, v, q and B in order to obtain a system which might govern solutions of the singular type sketched in figure 2 (and numerically found in figure 1). The main idea behind the derivation of the significant scaling is (again) the application of a 'jump' condition: a solution that leaves the slow manifold $\mathcal{M}$ in the neighbourhood of ℓ^U must return close to ℓ^S. This approach yields:

$$\begin{aligned} &\eta = \delta^{-\frac{1}{3}\alpha}\hat{\eta} \qquad u = \delta^{\alpha}\hat{u} \qquad p = \delta^{\frac{2}{3}\alpha}\hat{p} \qquad v = \frac{\hat{v}}{\delta^{\frac{1}{3}\alpha}} \\ &q = \hat{q} \qquad A = \delta^{2}a \qquad B = \delta^{\frac{2}{3}\alpha}b \qquad c = \delta^{1+\beta}\hat{\gamma}. \end{aligned} \tag{2.4}$$

We present the detailed derivation of this scaling analysis in the appendix.

Introducing these scalings into (1.4), and dropping hats, we arrive at:

$$\begin{aligned} \dot{u} &= \delta^{(1-\frac{2}{3}\alpha)}p \\ \dot{p} &= \delta^{(1-\frac{2}{3}\alpha)}[uv^2 - \delta^{(1+\beta+\frac{1}{3}\alpha)}\gamma p - \delta^{(2-\frac{1}{3}\alpha)}a + \delta^{(2+\frac{2}{3}\alpha)}au] \\ \dot{v} &= q \\ \dot{q} &= -uv^2 + bv - \delta^{(\beta-\frac{1}{3}\alpha)}\gamma q \end{aligned} \tag{2.5}$$

with two additional conditions for the free parameters α and β (see the appendix):

$$1 - \tfrac{2}{3}\alpha > 0 \qquad \text{or} \qquad 0 \leqslant \alpha < \tfrac{3}{2} \tag{2.6}$$

$$\beta - \tfrac{1}{3}\alpha \geqslant 2(1 - \tfrac{2}{3}\alpha) \qquad \text{or} \qquad \beta \geqslant 2 - \alpha > \tfrac{1}{2}. \tag{2.7}$$

In the next sections, we will expand the solutions of (2.5) with respect to the leading-order perturbation term $\delta^{(1-\frac{2}{3}\alpha)}$, and we will study the relative magnitudes of the 'friction' term in the fast field and the amplitude of the slow components of the vector field. Therefore, we introduce for simplicity of notation, ε and σ by

$$\varepsilon = \delta^{1-\frac{2}{3}\alpha} \qquad \text{and} \qquad \varepsilon^{2+\sigma} = \delta^{\beta-\frac{1}{3}\alpha}. \tag{2.8}$$

Furthermore, we define $\rho = \frac{1}{1-\frac{2}{3}\alpha}$, so that $\delta = \varepsilon^{\rho}$. Plugging in this final notation, the main equations to be analysed in this paper are:

$$\begin{cases} \dot{u} = \varepsilon p \\ \dot{p} = \varepsilon[uv^2 - \varepsilon^{\frac{1}{2}(3\rho+1)}a - \varepsilon^{(2\rho+1+\sigma)}\gamma p + \varepsilon^{(3\rho-1)}au] \\ \dot{v} = q \\ \dot{q} = -uv^2 + bv - \varepsilon^{(2+\sigma)}\gamma q. \end{cases} \tag{2.9}$$

Here, $0 < \varepsilon \ll 1$, $\sigma \geqslant 0$ and $\rho \geqslant 1$. Note that the critical point $S = (1, 0, 0, 0)$ of (1.4) has been rescaled into $(1/\delta^{\alpha}, 0, 0, 0)$ in (2.5) and $(1/\varepsilon^{\frac{3}{2}(\rho-1)}, 0, 0, 0)$ in (2.9), where we

remark that $\frac{3}{2}(\rho - 1) = \alpha\rho$. Also, for completeness, we note that σ is given explicitly by $\sigma = (\beta + \alpha - 2)/(1 - \frac{2}{3}\alpha)$.

Remark 2.1. Based on the numerical simulations shown in figure 1, those in section 6, and those of [22], one would say that α is approximately 1 in (2.5). In the simulations shown in figure 1, we took $\alpha = 1$ and $b = 0.6$; hence $B \approx 0.13$ in figure 1(a) and $B \approx 0.086$ in figure 1(b). Also, the choice $B = 0.079$ with $\delta^2 = 0.01$ in the numerical simulations of [22] is related to the realistic value of b of approximately 0.37, since, by (2.4), $B = 0.079 = b\delta^{2/3} \approx 0.366(0.01)^{1/3}$. However, in section 4 we shall see that there exist stationary pulses (thus $c = \gamma = 0$) for any $\alpha \in [0, \frac{3}{2})$. Nevertheless, the numerical simulations suggest that only those with $\alpha \approx 1$ can be stable (for certain values of a and b, see section 6). If we look for non-stationary (travelling) pulses, then the value of β becomes important, as we shall see in section 5. In the simulations illustrated in figures 7–9, we show numerically that the splitting pulses travel with speed $c = \mathcal{O}(\delta^2)$, thus, by (2.4), $\beta = 1$ in (2.5).

Remark 2.2. There are three free parameters in the original, unscaled system (1.4): A, B, γ. As a consequence of the scalings, there are five - $a, b, \gamma, \sigma, \rho$ - in (2.9) (or equivalently, $a, b, \gamma, \alpha, \beta$ in (2.5)). The main difference is that we introduced, by the scalings in this section, explicit new parameters that fixed the magnitudes of the parameters in (1.4) as order functions in δ by the scalings. All five parameters in (2.5) and (2.9) are $\mathcal{O}(1)$, which is clearly not the case in (1.4).

Remark 2.3. The above scaling respects the fundamental chemistry of the Gray–Scott model. Recall that $B = A + k_2$, where $k_2 > 0$. By our scaling, we see that B is always greater than A, since, by (2.4), $B = \delta^{2\alpha/3}b \gg A = \delta^2 a$ with $\alpha \in [0, \frac{3}{2})$ (see equation (2.9), for all a and b of $\mathcal{O}(1)$ and $0 < \delta \ll 1$).

Remark 2.4. In this section, the parameter $\alpha \in [0, \frac{3}{2})$ has been introduced by the observation that the solution U of (1.1) is not $\mathcal{O}(1)$ during a pulse excursion of V, but $\mathcal{O}(\delta^\alpha)$. On the other hand, one could also introduce α as the parameter that measures the magnitude of B with respect to δ: $B = \delta^{2\alpha/3}b$. From this point of view one can say that the magnitude of B determines the magnitude of U (and V) during a pulse-excursion (see also sections 6 and 7).

3. Global geometry for $\varepsilon = 0$ and for $0 < \varepsilon \ll 1$

The fast subsystem of (2.9) is given by

$$\begin{aligned} \dot{v} &= q \\ \dot{q} &= -uv^2 + bv - \varepsilon^{(2+\sigma)}\gamma q \end{aligned} \tag{3.1}$$

in which u is constant. When $\varepsilon = 0$, (3.1) is a one-parameter (u) family of planar Hamiltonian systems, with Hamiltonian

$$K(v, q; u) = \frac{q^2}{2} - \frac{b}{2}v^2 + \frac{1}{3}uv^3 \tag{3.2}$$

Moreover, when $\varepsilon = 0$, the equation (3.1) possesses a centre equilibrium at $(v = \frac{b}{u}, q = 0)$ and a saddle equilibrium at $(v = 0, q = 0)$ connected to itself by a homoclinic orbit (see figure 3(a))

$$v_0(t; u_0) = 3b/(2u_0)\,\mathrm{sech}^2[(\sqrt{b}/2)t] \qquad \text{and} \qquad q_0(t; u_0) = \dot{v}_0. \tag{3.3}$$

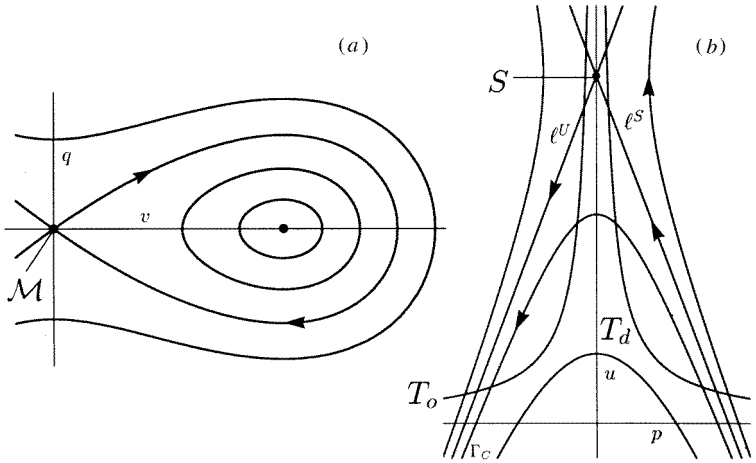

Figure 3. Schematic illustrations when $\gamma = 0$ of (*a*) the (v, q) phase space of the fast subsystem, and (*b*) the slow vector field on $\mathcal{M}$ for $\gamma = 0$ showing the location of the curves $T_{\rm o}$, $T_{\rm d}$, ℓ^U, ℓ^S, and a hyperbolic orbit segment Γ_C. Note that the u coordinates of the saddle, S, and the upper two intersections, $T_{\rm o} \cap \ell^U$ and $T_{\rm d} \cap \ell^S$, are only $\mathcal{O}(1)$ if $\alpha = 0$.

The homoclinic orbit, which may be thought of as a right-swimming fish, surrounds the centre equilibrium and is symmetric about the $v-$axis, with a maximum point at $(v_{\max} = \frac{3b}{2u}, q = 0)$. We shall frequently use the fact that v_0 is an even function of t.

The complete phase portrait of (2.9) when $\varepsilon = 0$ follows immediately by putting together the above geometrical information from the fast subsystem together with the simple observation that both variables u and p are constant in time when $\varepsilon = 0$ in (2.9). First, the plane $\mathcal{M} \equiv \{(u, p, v = 0, q = 0)\}$ is a normally hyperbolic manifold, trivially invariant since it is a plane of equilibria. Second, if we let U denote a large open set on $\mathcal{M}$ that contains the saddle equilibrium S but not points from the set $\{u = 0\}$, then the manifold $\mathcal{M}|_U$ has three-dimensional local stable and unstable manifolds. These three-dimensional manifolds are the unions of the one-dimensional local stable and unstable manifolds of the saddle equilibria of (3.1), and they are C^r smooth for every $r > 0$. Finally, each point $(u, p, v = 0, q = 0)$ on $\mathcal{M}$ is connected to itself by a homoclinic orbit. Therefore, the manifold $\mathcal{M}|_U$ is connected to itself by a three-dimensional homoclinic manifold $W(\mathcal{M})$.

3.1. Dynamics on $\mathcal{M}$

The detailed geometric information about the $\varepsilon = 0$ limit of (2.9) discussed above helps to determine the geometry of the full system (2.9). When $\varepsilon > 0$, the plane $\mathcal{M}$ is still invariant under the flow of the full system (2.9). The flow on $\mathcal{M}$ is slow, and most orbits on $\mathcal{M}$ leak out of U on the boundary in both forward and backward time.

When $\varepsilon > 0$, the slow subsystem

$$\begin{aligned} u' &= p \\ p' &= -\varepsilon^{\frac{1}{2}(3\rho+1)} a - \varepsilon^{(2\rho+1+\sigma)} \gamma p + \varepsilon^{(3\rho-1)} a u \end{aligned} \tag{3.4}$$

is linear and has precisely one saddle equilibrium at the restriction $S(u = 1/\varepsilon^{\frac{3}{2}(\rho-1)}, p = 0)$

of S to $\mathcal{M}$. The linearization of (3.4) has eigenvalues given by

$$\lambda_{\pm} \equiv \tfrac{1}{2}\varepsilon^{\frac{1}{2}(3\rho-1)}\left[\pm\sqrt{4a+\varepsilon^{(\rho+3+2\sigma)}\gamma^2}-\varepsilon^{\frac{1}{2}(\rho+3+2\sigma)}\gamma\right]. \tag{3.5}$$

Therefore, the stable and unstable manifolds of S restricted to $\mathcal{M}$ are known explicitly as graphs:

$$W^{U,S}(S)|_{\mathcal{M}} \stackrel{\text{def}}{=} \ell^{U,S}: \qquad p=\lambda_{\pm}\left(u-\frac{1}{\varepsilon^{\frac{3}{2}(\rho-1)}}\right) \tag{3.6}$$

where ℓ^U and ℓ^S are rescaled versions of (2.2) (see figure 3(*b*)). Asymptotically, we have:

$$\ell^{U,S}: \qquad p=\mp\varepsilon\sqrt{a}+\text{h.o.t.} \tag{3.7}$$

for $\alpha>0$ (equivalently $\rho>1$), $u=\mathcal{O}(1)$, independent of γ by (3.5). By contrast, when $\alpha=0$ (i.e. $\rho=1$), $\ell^{U,S}$ cannot be approximated by a vertical line '+ h.o.t.', and one must use (3.6).

3.2. Persistent fast connections

When $0<\varepsilon\ll 1$, the stable and unstable manifolds of $\mathcal{M}|_U$ in the $\varepsilon=0$ system persist as three-dimensional, C^r smooth stable and unstable manifolds, $W^U(\mathcal{M})$ and $W^S(\mathcal{M})$. This persistence result for the local manifolds follows from a straightforward application of the Fenichel theory of [7] to (2.9) (see also theorem 3 of [12]). The branches of these manifolds that coincided when $\varepsilon=0$ no longer do so, and in general will intersect each other in two-dimensional surfaces, and in these intersections lie the only orbits biasymptotic to $\mathcal{M}$.

We will employ a Melnikov method to detect these intersections. In particular, system (2.9) is of the type to which Robinson's extension of the Melnikov method applies, see [19, 24, 32]. Let $t\equiv\eta$, so that the independent variable of (2.9) is now denoted by t. Let $(u(t), p(t), v(t), q(t))$ represent a solution of (2.9) that passes through the point $(u_0, p_0, v(0), 0)$ at time $t=0$. Note that we have suppressed the ε dependence in this notation.

The splitting distance between the manifolds $W^U(\mathcal{M})$ and $W^S(\mathcal{M})$ can be measured in the hyperplane $\{q=0\}$, which is the hyperplane transverse to $W(\mathcal{M})$ and is spanned by the three vectors $(1,0,0,0)$, $(0,1,0,0)$, and the unit normal

$$\hat{n}\equiv\frac{(0,0,\frac{\partial K}{\partial v}(3b/2u,0;u),\frac{\partial K}{\partial q}(3b/2u,0;u))}{\|(0,0,\frac{\partial K}{\partial v}(3b/2u,0;u),\frac{\partial K}{\partial q}(3b/2u,0;u))\|}=(0,0,1,0). \tag{3.8}$$

The distance measurement is given by

$$\Delta K(u_0,p_0;a,b,\gamma)\equiv\int_{-\infty}^{\infty}\dot{K}(v(t),q(t);u(t),p(t))\,\mathrm{d}t \tag{3.9}$$

as $\varepsilon\to 0^+$, where a straightforward computation yields

$$\dot{K}=-\varepsilon^{(2+\sigma)}\gamma q^2+\tfrac{1}{3}\varepsilon p v^3. \tag{3.10}$$

Since we look for solutions on these perturbed stable and unstable manifolds $W^S(\mathcal{M})$ and $W^U(\mathcal{M})$, we need to expand the solutions $(u(t), p(t), v(t), q(t))$ of (2.9) in powers of the small parameter ε. The structure of this expansion will depend on the values of σ and

ρ. However, we note that the expansion remains standard at least up to terms smaller than $\mathcal{O}(\varepsilon^2)$:

$$\begin{aligned} u(t) &= u_0 + \varepsilon u_1(t) + \varepsilon^2 u_2(t) + \text{h.o.t.} \\ p(t) &= p_0 + \varepsilon p_1(t) + \varepsilon^2 p_2(t) + \text{h.o.t.} \\ v(t) &= v_0(t; u_0) + \varepsilon v_1(t) + \varepsilon^2 v_2(t) + \text{h.o.t.} \\ q(t) &= q_0(t; u_0) + \varepsilon q_1(t) + \varepsilon^2 q_2(t) + \text{h.o.t.} \end{aligned} \tag{3.11}$$

as $\varepsilon \to 0$, where $v_0(t; u_0)$ and $q_0(t; u_0)$ are the unperturbed homoclinic solutions given in (3.3). Note that it depends on σ whether the next term in the expansion of $v(t)$ is of $\mathcal{O}(\varepsilon^{(2+\sigma)})$ or $\mathcal{O}(\varepsilon^3)$. This distinction will become important in section 5. Solutions on the local unstable manifold of $\mathcal{M}$ are represented by expansions valid on the semi-infinite time interval $(-\infty, 0]$, and solutions on the local stable manifold of $\mathcal{M}$ are represented by expansions valid on the semi-infinite time interval $[0, -\infty)$. The higher-order terms will be determined perturbatively.

We choose the initial conditions on the curve $W^S(\mathcal{M}) \cap W^U(\mathcal{M}) \cap \{q = 0\}$, whose existence we establish below. We assume that $u(0) = u_0$ and $u_j(0) = 0$ for $j \geqslant 1$: the initial conditions p_0, $p_j(0)$ and $v_j(0)$ ($j \geqslant 1$) are then determined as a function of u_0 by the condition that $\Gamma(t) = (u(t), p(t), v(t), q(t)) \in W^S(\mathcal{M}) \cap W^U(\mathcal{M})$.

Remark 3.1. In this type of Melnikov calculation, it is usually sufficient to use only the unperturbed solution $(u_0, p_0, v_0(t; u_0), q_0(t; u_0))$. However, here we need higher-order corrections since the magnitude of the perturbation in the fast field, $\mathcal{O}(\varepsilon^{(2+\sigma)})$, is smaller than the evolution of the slow field, $\mathcal{O}(\varepsilon)$.

By substituting (3.11) into (2.9), we find for the first-order corrections of u and p:

$$\begin{aligned} u_1(t) &\equiv 0 \\ p_1(t) &= \int_0^t u_0 v_0^2(\tau)\, \mathrm{d}\tau + p_1(0). \end{aligned} \tag{3.12}$$

Note that the integral term in $p_1(t)$ is an odd function of the time variable t. Determining $v_1(t)$ and all other higher-order terms depends on the type of solutions one is looking for and requires further analysis. Plugging these expansions into (3.10) and (3.9) yields:

$$\Delta K = \varepsilon \int_{-\infty}^{\infty} [\tfrac{1}{3} p_0 v_0^3(t) + \varepsilon(\tfrac{1}{3} p_1(t) v_0^3(t) + p_0 v_0^2(t) v_1(t) - \varepsilon^\sigma \gamma q_0^2(t)) + \text{h.o.t.}]\, \mathrm{d}t \tag{3.13}$$

where ΔK is a function of u_0, p_0; and the parameters a, b, and γ.

We consider solutions that are biasymptotic to $\mathcal{M}$; thus, ΔK must have zeroes, and there must be a balance between some of the terms in the integrand. Moreover, these solutions must be homoclinic to S; and, hence, they take off (respectively, touch down) from (on) $\mathcal{M}$ near ℓ^U (ℓ^S). Thus, by (3.7) and the fact that the perturbations can at most have an $\mathcal{O}(\varepsilon)$ influence on $p(t)$ during half a circuit through the fast field, we have to set $p_0 = 0$ and $p_1(0) = \hat{p}_0$; i.e. $\hat{p}_0$ determines the initial condition of $p(t)$ at the $\mathcal{O}(\varepsilon)$ level. Moreover, we observe that $\Delta K = \mathcal{O}(\varepsilon^2)$, and hence $|v(0) - v_0(0)| = \mathcal{O}(\varepsilon^2)$. Thus, the first-order correction v_1 of v is a solution of a homogeneous second-order linear equation with initial conditions $v_1(0) = \dot{v}_1(0) (= q_1(0)) = 0$, namely: $v_1(t) \equiv 0$. Now, we recall from (3.12) that the integral term in $p_1(t)$ is odd and also that $v_0(t)$ is even, so that all parts of the second term in the integrand of (3.13), except the function $p_1(0) v_0^3(t)$, are odd. Hence, (3.13) reduces to:

$$\Delta K(u_0, p_0; a, b, \gamma) = \varepsilon^2 \int_{-\infty}^{\infty} (\tfrac{1}{3} \hat{p}_0 v_0^3(t) - \varepsilon^\sigma \gamma q_0^2(t))\, \mathrm{d}t + \text{h.o.t.}$$

Using (3.3), a straightforward integration yields:

$$\Delta K(u_0, p_0; a, b, \gamma) = \varepsilon^2 \left(\frac{6b^2\sqrt{b}}{5u_0^2} \right) \left(\frac{2\hat{p}_0}{u_0} - \varepsilon^\sigma \gamma \right) + \text{h.o.t.} \tag{3.14}$$

Therefore, to leading order, ΔK has simple zeroes along the line

$$p = \tfrac{1}{2}\varepsilon^{(1+\sigma)}\gamma u. \tag{3.15}$$

This result should be interpreted as follows: the orbits $\Gamma(t; x_0)$ through the points $x_0 = (u, p, v_0(0; u), 0)$ are biasymptotic to $\mathcal{M}$ if u and p are related to leading order as in (3.15). Note that it has now become clear that σ cannot become negative, or, in the terminology of (2.5), that $\beta - \frac{1}{3}\alpha$ cannot be smaller than $2(1 - \frac{2}{3}\alpha)$ (the scalings in (2.3) imply that both u $(= \hat{u})$ and γ $(= \hat{\gamma})$ are exactly $\mathcal{O}(1)$ with respect to ε, while p cannot be larger than $\mathcal{O}(\varepsilon)$ by (3.7)).

In order to quantify the influence of the fast field on the u- and p-coordinates of a solution in $W^U(\mathcal{M}) \cap W^S(\mathcal{M})$ during its excursion through the fast field, we define

$$\Delta p(u_0, p_0; a, b, \gamma) \equiv \int_{-\infty}^{\infty} \dot{p}\, \mathrm{d}t \tag{3.16}$$

$$\Delta u(u_0, p_0; a, b, \gamma) \equiv \int_{-\infty}^{\infty} \dot{u}\, \mathrm{d}t. \tag{3.17}$$

Straightforward computations give (by (2.9) where $\rho \geqslant 1$):

$$\begin{aligned} \Delta p &= \varepsilon \int_{-\infty}^{\infty} (u(t)v^2(t) + \mathcal{O}(\varepsilon^2)))\, \mathrm{d}t \\ &= \varepsilon \int_{-\infty}^{\infty} [u_0 v_0^2(t) + \varepsilon(u_1(t)v_0^2(t) + 2u_0 v_0(t)v_1(t)) + \mathcal{O}(\varepsilon^2)]\, \mathrm{d}t \\ &= \varepsilon \frac{6b\sqrt{b}}{u_0} + \mathcal{O}(\varepsilon^3) \end{aligned} \tag{3.18}$$

where we have again used $u_1(t) = 0$ and $v_1(t) = 0$. Finally, we use the fact that we will only study $\Delta u(u_0, p_0)$ for values of (u_0, p_0) in the neighbourhood of the $\Delta K = 0$ line (3.15). Thus, $p_0 = \mathcal{O}(\varepsilon)$ which yields by (2.9) that the change in u is of higher order:

$$\Delta u = \mathcal{O}(\varepsilon^2). \tag{3.19}$$

There are two other curves on $\mathcal{M}$ that play a crucial role in the analysis of the next sections and that are obtained as follows. The first intersection of $W^S(\mathcal{M})$ and $W^U(\mathcal{M})$ in the hyperplane $\{q = 0\}$ is given by (3.15) to leading order. This intersection is a one-dimensional curve in the two-dimensional manifold $W^S(\mathcal{M}) \cap W^U(\mathcal{M})$. Through any point x_0 on this curve $W^S(\mathcal{M}) \cap W^U(\mathcal{M}) \cap \{q = 0\}$ there is an orbit $\Gamma(t; x_0)$ which approaches $\mathcal{M}$ for 'large' t. More precisely, the Fenichel theory [7] already cited above implies that for any $\Gamma(t; x_0)$ there are two orbits $\Gamma^+_{\mathcal{M}} = \Gamma^+_{\mathcal{M}}(t; x_0^+) \subset \mathcal{M}$ and $\Gamma^-_{\mathcal{M}}(t; x_0^-) \subset \mathcal{M}$, respectively (where $\Gamma^+(0, x_0^+) = x_0^+ \in \mathcal{M}$), such that $\|\Gamma(t; x_0) - \Gamma^+_{\mathcal{M}}(t; x_0^+)\|$ is exponentially small for $t > 0$ where $t \geqslant \mathcal{O}(\frac{1}{\varepsilon})$ and $\|\Gamma(t; x_0) - \Gamma^-_{\mathcal{M}}(t; x_0^-)\|$ is exponentially small for $t < 0$ with $-t \geqslant \mathcal{O}(\frac{1}{\varepsilon})$. As a consequence,

$$\mathrm{d}(\Gamma(t; x_0), \mathcal{M}) = \mathcal{O}(\mathrm{e}^{-\frac{k}{\varepsilon}}) \qquad \text{for } |t| \geqslant \mathcal{O}\left(\frac{1}{\varepsilon}\right) \text{ or larger}$$

for some $k > 0$, and $\Gamma^\pm_{\mathcal{M}}(t; x_0^\pm)$ determine the behaviour of $\Gamma(t; x_0)$ near $\mathcal{M}$. Therefore, we define the curves $T_\mathrm{o} \subset \mathcal{M}$ (take off) and $T_\mathrm{d} \subset \mathcal{M}$ (touch down) as

$$T_\mathrm{o} = \cup_{x_0}\{x_0^- = \Gamma^-_{\mathcal{M}}(0; x_0^-)\} \qquad \text{and} \qquad T_\mathrm{d} = \cup_{x_0}\{x_0^+ = \Gamma^+_{\mathcal{M}}(0; x_0^+)\} \tag{3.20}$$

where the unions are over all x_0 in $W^S(\mathcal{M}) \cap W^U(\mathcal{M}) \cap \{q = 0\}$. T_o (respectively T_d), is the collection of base points of all of the fibres in $W^U(\mathcal{M})$ (respectively $W^S(\mathcal{M})$) that lie in the transverse intersection of $W^U(\mathcal{M})$ and $W^S(\mathcal{M})$. See figure 3(b) for a diagram when $\gamma = 0$.

The locations of T_o and T_d can be obtained explicitly by determining the relations between $x_0 = (u_0, p_0, v_0, 0)$ and $x_0^{\pm} = (u_0^{\pm}, p_0^{\pm}, 0, 0)$. The accumulated change in p of $\Gamma(t)$ during the (half-circuit) excursion through the fast field is measured by

$$\int_{-\infty}^{0} \dot{p}\, \mathrm{d}t \qquad \text{and} \qquad \int_{0}^{\infty} \dot{p}\, \mathrm{d}t$$

when $t < 0$ and $t > 0$, respectively. The changes in p of $\Gamma^{\pm}(t)$ during the same period of time can be neglected, in highest orders, since $\dot{p} = \mathcal{O}(\varepsilon^3)$ on $\mathcal{M}$ by (2.9). By (2.9) and (3.19), we also conclude that $u_0 = u_0^{\pm}$ to leading order. Since x_0 is given by (3.15), we find (by a calculation similar to (3.18)) to leading order:

$$\begin{aligned} T_o: &\qquad p = \frac{1}{2}\varepsilon\left(\varepsilon^{\sigma}\gamma u - \frac{6b\sqrt{b}}{u}\right) \\ T_d: &\qquad p = \frac{1}{2}\varepsilon\left(\varepsilon^{\sigma}\gamma u + \frac{6b\sqrt{b}}{u}\right). \end{aligned} \tag{3.21}$$

Having identified in this section the geometric features of (2.9) both in the invariant plane $\mathcal{M}$ and in the directions transverse to it, we are now ready to construct the stationary waves of (1.1). However, we will see in section 5 that a more subtle analysis is necessary in order to study the (non-)existence of travelling waves.

4. Stationary solutions

In this section, we focus on the stationary ($c = 0$) solutions of (1.1). These are given by solutions of (2.9) with $\gamma = 0$. In particular, for $\alpha \in (0, \frac{3}{2})$, we construct single-pulse and multi-pulse orbits homoclinic to S in section 4.1, as well as a variety of multi-pulse periodic solutions, including the steady states reported in the simulations of [22], in section 4.2. The special case of $\alpha = 0$ is treated in section 4.3. Finally, we refer the reader to section 6 for the results of numerical simulations in which many of these homoclinic and periodic stationary waves are observed as stable patterns.

4.1. Single-pulse and multi-pulse homoclinic orbits

When $\gamma = 0$, the equations (2.9) possess the symmetry:

$$t \to -t \qquad p \to -p \qquad \text{and} \qquad q \to -q. \tag{4.1}$$

One-pulse homoclinic orbits of the type described in section 2 are constructed as follows (see figure 2(a)). Let $\Gamma^-(t) = (u^-(t), p^-(t), v^-(t), q^-(t))$ denote an orbit of (2.9) on $W^U(S)$ with $v^-(t) > 0$. Its existence guarantees the existence of a symmetric solution on $W^S(S)$ which we denote:

$$\Gamma^+(t) = (u^+(t), p^+(t), v^+(t), q^+(t)) = (u^-(-t), -p^-(-t), v^-(-t), -q^-(-t)).$$

For large negative t, Γ^- lies close to $\mathcal{M}$ and moves along ℓ^U as t increases. Γ^- leaves the neighbourhood of $\mathcal{M}$ in an $\mathcal{O}(\varepsilon)$ ball about a take-off point (u_0^-, p_0^-) on $\ell^U \cap T_o$, where u_0 is $\mathcal{O}(1)$ and will be determined below. Then, Γ^- makes an excursion through the

fast vector field and transversely intersects the $\{q = 0\}$ hyperplane for the first time in a point which we shall denote (u_1, p_1, v_1). By the symmetry (4.1), Γ^+ executes a symmetric trajectory in backward time: it departs ℓ^S in an $\mathcal{O}(\varepsilon)$ ball about the touch down point $(u_0^+, p_0^+) = (u_0^-, -p_0^-) \in \mathcal{M}$ and transversely intersects the $\{q = 0\}$ hyperplane for the first time in the point $(u_1, -p_1, v_1)$. One-pulse solutions therefore exist when $p_1 = 0$, so that the two intersection points coincide. In that case, $\Gamma^-(t) = \Gamma^+(t) \in W^U(S) \cap W^S(S)$ is the one-pulse homoclinic orbit.

We proceed to compute p_1. From section 3, we know that $p_1 = p_0^- + \frac{1}{2}\Delta p$ where Δp is the increment in p during half an excursion in the fast field and is given by (3.18): $\Delta p = \varepsilon \frac{6b\sqrt{b}}{u_0^-} + \text{h.o.t.}$. Note that Δp has been computed in section 3 for orbits $\Gamma(t)$ with $\Gamma(0) \in \{q = 0, v > 0\}$ and that we replaced u_0, the u-coordinate of $\Gamma(0)$ in (3.18), by u_0^-. However, we observe by (3.19) that $u_0^- = u_0^+ = u_0 + \mathcal{O}(\varepsilon^2)$. We infer from (3.7) that $p_0^- = -\varepsilon\sqrt{a} + \text{h.o.t.}$ for $(u_0^-, p_0^-) \in \ell^U$. Hence, p_1 is a function of u_0^-; and, setting $p_1 = 0$ to leading order yields:

$$u_0^- = 3b\sqrt{\frac{b}{a}}. \tag{4.2}$$

Thus, we have proved the following theorem for the case $N = 1$.

Theorem 4.1. *There exists an $\varepsilon_0(\alpha) > 0$ such that for every $0 < \varepsilon < \varepsilon_0(\alpha)$, for $\alpha \in (0, \frac{3}{2})$, for every a and $b > 0$, and for every positive integer N, the system (2.9) with $\gamma = 0$ possesses a unique N-pulse orbit homoclinic to S. Moreover, for each N, the homoclinic orbit consists of two slow segments interspersed with N successive excursions in the fast field during which u is near $3Nb\sqrt{b/a}$. Finally, for each N, the homoclinic orbit lies in the transverse intersection of $W^U(S)$ and $W^S(S)$.*

Remark 4.1. Note that the above calculation with (3.7) is only possible for $\alpha > 0$ or, equivalently $\rho > 1$. In fact, $\varepsilon_0(\alpha) \to 0$ as $\alpha \to 0$. The case $\alpha = 0$ is special. In this case, (2.9) reduces to the unscaled (1.4) with $A = \delta^2 a$ (use (2.4)). Moreover, one has to use (3.6) instead of (3.7). In section 4.3, we will establish (theorem 4.3) that when $\alpha = 0$ there can be either two or zero homoclinic orbits (with a saddle node bifurcation of homoclinic orbits in between), depending on the values of a and b. See also the discussion after theorem 4.3 as well as that in remark 2.2.

Proof of theorem 4.1. Note that the last statement of the theorem follows directly from the dependence of Δp on u_0^-. Since Δp depends inversely on u_0^-, (4.2) is a simple zero of p_1. Hence, the symmetry (4.1) implies that $W^U(S)$ and $W^S(S)$ intersect transversely in this homoclinic orbit. We remark that these same results for $\gamma = 0$ can be obtained (section 5) by considering the general case $\gamma \geqslant 0$, and examining the intersection of T_o and ℓ^U as given by (3.21) and (3.7), respectively.

We proceed to prove the theorem for $N \geqslant 2$, again relying heavily on the symmetry (4.1). See figure 4 for an illustration of an N-pulse orbit with $N = 2$. First, we construct the two-pulse orbit. Consider a solution $\Gamma^-(t)$ on $W^U(S)$ that intersects the hyperplane $\{q = 0\}$ a second time at the point (u_2, p_2, v_2). Such a solution exists as long as ε is sufficiently small and the take-off point (u_0^-, p_0^-) can be chosen such that $\Delta K < 0$, so that $\Gamma^-(t)$ is neither in the local stable manifold of $\mathcal{M}$ nor winds up on the other side of $W^S(\mathcal{M})$ (that is: $v^-(t)$ does not become negative immediately after the (first) return of Γ^- to an $\mathcal{O}(\sqrt{\varepsilon})$ neighbourhood of $\mathcal{M}$). We show at the end of this construction that this choice is possible.

Due to the symmetry (4.1), $\Gamma^+(t)$ also has a second transverse intersection with the hyperplane $\{q = 0\}$ at the point $(u_2, -p_2, v_2)$. The semi-orbits $\Gamma^-(t)$ and $\Gamma^+(t)$ hook up if $p_2 = 0$. Hence, it remains to calculate $p_2 = p_0^- + \Delta p$, where Δp is a change in p during

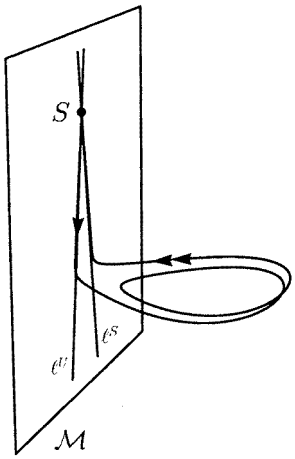

Figure 4. Schematic illustration of the $N = 2$ pulse homoclinic orbit of (2.9).

one complete circuit in the fast field (3.18). Recalling (2.9) and the fact that $p \leqslant \mathcal{O}(\varepsilon)$ over the time interval of interest, or equivalently, by using (3.19), we see that u remains constant to sufficiently high order during both of the near-separatrix excursions that this two-pulse orbit makes. Hence, this two-pulse orbit departs from $\mathcal{M}$ in an $\mathcal{O}(\varepsilon)$ ball centred at the point (u_0^-, p_0^-) with

$$u_0^- = 6b\sqrt{\frac{b}{a}} \tag{4.3}$$

exactly as stated in the theorem. The fact that this two-pulse homoclinic orbit lies in the transverse intersection of $W^U(S)$ and $W^S(S)$ follows directly from the symmetry (4.1) and the fact that p_2 has a simple zero at $u_0^- = 6b\sqrt{b/a}$. For the sake of completion, we observe that $v_2 = \mathcal{O}(\sqrt{\varepsilon})$ since $\Delta K = \mathcal{O}(\varepsilon)$.

Inductively, one uses the same procedure to construct N-pulse homoclinic orbits for any finite $N > 2$. Of course, one must ascertain, as we do below, that $\Delta K < 0$ after $\Gamma^-(t)$ has made its $(N-1)$th near-separatrix excursion, so that this orbit always stays on the correct side of $W^S(\mathcal{M})$. We find that these $N-$pulse orbits leave $\mathcal{M}$ near (u_0^-, p_0^-), where:

$$u_0^- = 3Nb\sqrt{\frac{b}{a}} \tag{4.4}$$

and that p_N has a simple zero at u_0^-.

Finally, we establish that the orbits Γ^- which return to the hyperplane $\{q = 0\}$ finitely many times, whose existence we assumed in the above constructions for $N \geqslant 2$, do indeed exist. Recalling (3.14), we see that $\Delta K < 0$ for orbits with $p_0 < 0$ and $\gamma = 0$, where p_0 is the p-coordinate of the intersection of $\Gamma(t)$ with the hyperplane $\{q = 0, v > 0\}$. Hence, each time $\Gamma^-(t)$ departs from a neighbourhood of $\mathcal{M}$ to the left of the take-off curve, T_o, it always intersects the hyperplane $\{q = 0\}$ another time with $v = \mathcal{O}(1)$ (see figure 3(*b*)). For values of u_0^- greater than $u_0^- = 3b\sqrt{b/a} \in \ell^U \cap T_o$ corresponding to the one-pulse homoclinic, we know that ℓ^U is to the left of T_o, thus $\Gamma^-(t)$ will at least intersect $\{q = 0\}$ three times: twice for $v = \mathcal{O}(1)$, once in between for $0 < v \ll 1$. A straightforward calculation shows that a second intersection of $\Gamma^-(t)$ with $\{q = 0\}$ $\mathcal{O}(\sqrt{\varepsilon})$ near $\mathcal{M}$ is only possible for $u_0^- \geqslant 9b\sqrt{b/a} + \mathcal{O}(\varepsilon)$. Thus, the three-pulse homoclinic orbit constructed above plays the role of separatrix solution. Inductively, one can show along the same lines that each of the $N = (2n-1)$-pulse solutions is a separatrix solution and that it is only

possible for $\Gamma^-(t)$ to have an nth intersection with the hyperplane $\{q = 0\}$ $\mathcal{O}(\sqrt{\varepsilon})$ near $\mathcal{M}$ if $u_0^- \geqslant 3(2n-1)b\sqrt{b/a} + \mathcal{O}(\varepsilon)$. This completes the proof of theorem 4.1. □

Remark 4.2. The result of theorem 4.1 can be generalized to obtain homoclinic orbits with N pulses where $N = o(1/\varepsilon)$. To show this, we consider an N of $\mathcal{O}(\varepsilon^{-s})$, for a certain $s > 0$. Errors in Δu and Δp have become $\mathcal{O}(\varepsilon^{2-s})$ after $\mathcal{O}(\varepsilon^{-s})$ circuits through the fast field. This expression has to remain smaller than the leading order term of $\mathcal{O}(\varepsilon)$. However, during each excursion in the fast field, the increment in p is $\mathcal{O}(\varepsilon)$, so we conclude that the above analysis is valid for $N = \mathcal{O}(\varepsilon^{-s})$ with $s < 1$.

4.2. Periodic steady states

In this section, we construct a variety of periodic steady states ($c = 0$), including those observed in the numerical simulations, see figure 1 of [22], and section 6 of this work. The simulations of [22] were performed on an interval with periodic boundary conditions. An initially solitary pulse replicated until it filled the interval with eight identical, stationary, pulses. In section 6, we will show that such a periodic pattern also occurs on unbounded domains, at the core of the self-replicating pulse pattern. The $M-$pulse periodic orbits observed in the simulations consist of M copies of the same fundamental periodic orbit in the (u, p, v, q) phase space. This fundamental orbit consists of one fast excursion from the slow manifold $\mathcal{M}$ and one (long) segment during which the orbit is near $\mathcal{M}$. Thus, v and q are exponentially small during the largest part of the period, which yields that the solution V of the PDE (1.1) must have the same behaviour (see section 6). We prove the existence of various families of such fundamental periodic orbits. Moreover, we are able to calculate the period and other key features of these orbits, so that we can explicitly determine the fundamental orbit corresponding to a numerically observed stationary periodic pattern.

In order to carry out the construction, we focus on the special case of $\alpha = 1$ in (2.9), which corresponds to the numerically observed steady states. The same analysis can be done, however, for all $\alpha \in (0, \frac{3}{2})$, and in the proof below we show how to extend the $\alpha = 1$ results to all these α. For $\alpha = 1$, the slow vector field on $\mathcal{M}$ is

$$\begin{aligned} \dot{u} &= \varepsilon p \\ \dot{p} &= \varepsilon^9 a u - \varepsilon^6 a \end{aligned} \tag{4.5}$$

which is simply (2.9) with $\gamma = 0$, $\rho = 3$ and $(v, q) = (0, 0)$. This slow system is linear with a saddle fixed point at $S = (1/\varepsilon^3, 0)$, and all orbits Γ_C are branches of hyperbolas given by

$$\left(\frac{1}{\varepsilon^3} - u\right)^2 - \frac{p^2}{\varepsilon^8 a} = C \tag{4.6}$$

parametrized by C (see figure 3(b)). Here, we are interested in the orbits Γ_C in the sector below S with $C > 0$, that is, the area enclosed by ℓ^U and ℓ^S, as defined in section 3.1. These orbits are symmetric about the $u-$axis, and for each such orbit segment, there exists a maximum value $u_{\max}$ of u such that $(u, p) = (u_{\max}, 0)$ is the symmetry point. Instead of C, $u_{\max}$ can also be used to parametrize the orbits Γ_C (4.6):

$$p^2 = \varepsilon^2 a[(1 - \varepsilon^3 u)^2 - (1 - \varepsilon^3 u_{\max})^2] \qquad \text{with } C = \left(\frac{1}{\varepsilon^3} - u_{\max}\right)^2. \tag{4.7}$$

Note that the lines $\ell^{U,S}$ correspond to $C = 0$ or $u_{\max} = 1/\varepsilon^3$, the u-coordinate of the saddle S; also, $C > 0$ corresponds to $u_{\max} < 1/\varepsilon^3$.

The orbits Γ_C can intersect the take-off and touch-down curves T_o and $T_d \subset \mathcal{M}$ (see figure 3(*b*)). Below, we will show that there exist periodic solutions to (2.9) which 'start' at $t = 0$ exponentially close to $(u_{\max}, 0, 0, 0) \in \mathcal{M}$ and follow Γ_C downwards to an intersection $\Gamma_C \cap T_o$, then take off for a circuit through the fast field after which they again touch down on $\mathcal{M}$ near $\Gamma_C \cap T_d$ and follow Γ_C upwards to 'end' on its initial point near $(u_{\max}, 0, 0, 0)$. However, first we need to pay some attention to the intersections $\Gamma_C \cap T_o$, or symmetrically, $\Gamma_C \cap T_d$. *A priori*, one would guess that T_o might intersect Γ_C more than once. Using expressions (3.21) and (4.7) it is easy to determine values for $u_{\max}$ such that T_o intersects Γ_C twice, but, the u-coordinates of these intersections can never both be $\mathcal{O}(1)$ (unless $\alpha = 0$, see section 4.3). This is a crucial point: if the u-coordinate of a take off point is not $\mathcal{O}(1)$, then the analysis of section 3 is not valid, since all coefficients of the ε-expansions in that section are (implicitly) assumed to be $\mathcal{O}(1)$. Moreover, system (2.9) is determined such that the excursions through the fast field take place for $u = \mathcal{O}(1)$, by construction. Thus, the expression (3.21) is only valid when u is $\mathcal{O}(1)$; and, the intersections $\Gamma_C \cap T_o$ with $u > \mathcal{O}(1)$ must be treated as $\mathcal{O}(1)$ intersections for a different scaling of u, or better, $\hat{u}$. In other words: the $u > \mathcal{O}(1)$ intersections of (3.21) and (4.7) are described by (2.9) with $\alpha < 1$, since we chose $\alpha = 1$ above.

It is clear from the combination of (3.21) and (2.9) that an intersection with $u = \mathcal{O}(1)$ is only possible for $u_{\max} = \mathcal{O}(1/\varepsilon^3)$. Thus, we introduce the new $\mathcal{O}(1)$ parameter $U_{\max}$ by

$$u_{\max} = \frac{U_{\max}}{\varepsilon^3} \qquad U_{\max} \leqslant 1. \tag{4.8}$$

It follows from (4.7) and (3.21) that $\Gamma_C \cap T_o$ (with $\gamma = 0$) is given to leading order by

$$(u_P, p_P) = (u_P(U_{\max}), p_P(U_{\max})) = \left(\frac{3b\sqrt{b}}{\sqrt{a(2U_{\max} - U_{\max}^2)}}, -\varepsilon\sqrt{a(2U_{\max} - U_{\max}^2)} \right) \tag{4.9}$$

which we simply denote (u_P, p_P). Note that (4.9) coincides with (4.2) and (3.7) as $U_{\max} \uparrow 1$, this is necessary since Γ_C merges with $\ell^U \cup \ell^S$ in this limit (see figure 2(*b*)). We can formulate the main result of this subsection.

Theorem 4.2. *For every ε sufficiently small, $\alpha \in (0, \frac{3}{2})$ and for any $U_{\max} < 1$ of $\mathcal{O}(1)$, the system (2.9) with $\gamma = 0$ possesses a periodic orbit which consists of two distinguished parts: a slow part near $\Gamma_C \in \mathcal{M}$ for $u > u_P$ (4.9) and an excursion through the fast field near the $\{u = u_P\}$ hyperplane.*

Remark 4.3. So far, we only considered the case $\alpha = 1$. All of the above is also valid for any $\alpha \in (0, \frac{3}{2})$ (with u_P exactly as in (4.9)). In section 4.3, we will discuss the special case $\alpha = 0$.

Proof of theorem 4.2. We fix an arbitrary value of $U_{\max} < 1$, which automatically determines a value of C, see (4.7). We recall from section 3 that, for every orbit $\Gamma_h(t, x_0)$ of (2.9) that is homoclinic to $\mathcal{M}$ and that passes through the point x_0 in the first intersection of $W^S(\mathcal{M})$ and $W^U(\mathcal{M})$ in the hyperplane $\{q = 0\}$, there exist orbits on $\mathcal{M}$, denoted by $\Gamma^{\pm}_{\mathcal{M}}(t; x_0^{\pm})$, such that $\|\Gamma_h(t; x_0) - \Gamma^{\pm}_{\mathcal{M}}(t; x_0^{\pm})\| = \mathcal{O}(\mathrm{e}^{-k/\varepsilon})$ for $|t| = \mathcal{O}(1/\varepsilon)$. Among this family of homoclinic orbits, there exists a unique one, which we denote $\Gamma_{h,C}(t; x_0)$, whose associated take-off and touch-down points $x_0^- \equiv \Gamma^-_{C,\mathcal{M}}(0; x_0^-)$ and $x_0^+ \equiv \Gamma^+_{C,\mathcal{M}}(0; x_0^+)$ lie precisely on $\Gamma_C \cap T_o$ and $\Gamma_C \cap T_d$, respectively, where $x_0^{\pm} = (u_P, \mp p_P, 0, 0)$ (4.9), due to the symmetry (4.1). Also, x_0^- is the forward image of x_0^+ under the flow of (4.5), since both points lie on Γ_C. In other words, the orbits Γ_C, $\Gamma^-_{C,\mathcal{M}}$, and $\Gamma^+_{C,\mathcal{M}}$ are 'time' translates of each other. For completeness, we note that the complete orbit, $\Gamma_{h,C}$, homoclinic to $\mathcal{M}$

(not S) passes through an exponential neighbourhood of $\Gamma_C \cap \{u > u_P\}$ twice and its u and p coordinates are unbounded for $t \to \pm\infty$.

We now show that there exists a periodic orbit $\Gamma_P(t)$ of the type described in the theorem, whose slow segments are exponentially close to $\Gamma_{h,C} \cap \{u > u_P\}$. Consider the line segment ℓ of points $(u_{\max}, 0, v, 0)$ such that the v coordinate satisfies $K_1 \exp[-(k/\varepsilon^5)] \leqslant v \leqslant K_2 \exp[-(k/\varepsilon^5)]$ for sufficiently small K_1, sufficiently large K_2, and for some $k > 0$, and all three constants are $\mathcal{O}(1)$. Note that the time of flight from $u = u_{\max}$ to $u = \mathcal{O}(1)$ along Γ_C is $\mathcal{O}(\varepsilon^{-5})$. Flowing the initial conditions on ℓ forward generates a two-dimensional manifold $\mathcal{L}$. Furthermore, with the constants k, K_1, and K_2 chosen appropriately, some of the orbits on $\mathcal{L}$ exit an $\mathcal{O}(\varepsilon)$ neighbourhood of $\mathcal{M}$ near Γ_C with $u > u_P$ and some exit with $u < u_P$. Finally, at these exit points, $\mathcal{L}$ is C^1-$\mathcal{O}(\exp[-(c/\varepsilon^5)])$ close to the invariant foliation on $W^U(\mathcal{M})$ with base points restricted to Γ_C. This closeness estimate follows from the modified version (see [27]) of the exchange lemma with an exponentially small error of [13]. The first application of the theory of the exchange lemma to find periodic orbits in singularly perturbed systems is given in [27]. Of course, by the symmetry (4.1), these same arguments show that $\mathcal{L}$ also lies C^1-$\mathcal{O}(\exp[-(c/\varepsilon^5)])$ close to $W^S(\mathcal{M}|_{\Gamma_C})$ at points at which orbits on $\mathcal{L}$ exit an $\mathcal{O}(\varepsilon)$ neighbourhood of $T_{\mathrm{d}} \cap \ell^S \in \mathcal{M}$ in backward time. Therefore, since $W^U(\mathcal{M})$ and $W^S(\mathcal{M})$ intersect transversely, so must $\mathcal{L}$ intersect itself transversely, exponentially close to the above constructed orbit, $\Gamma_{h,C}$. Moreover, due to the transversality of the intersections $T_{\mathrm{o}} \cap \Gamma_C$ and $T_{\mathrm{d}} \cap \Gamma_C$, this intersection of $\mathcal{L}$ with itself is locally unique, and therefore so is the periodic orbit Γ_P that lies inside it.

To conclude the proof of the theorem, we briefly consider the case $\alpha \neq 1$ ($\alpha > 0$). The idea of the proof in this case is in essence the same, one only has to adapt the length of the line segment ℓ since the 'time of flight' from $u_{\max}$ ($= \mathcal{O}(1/\varepsilon^{3/2(\rho-1)})$) to $u = \mathcal{O}(1)$ depends on α (or ρ). □

Finally, we exploit the fact that the flow on $\mathcal{M}$ is linear to explicitly calculate the leading order length of the period of a periodic orbit $\Gamma_P(t)$. Since we want to apply the outcome to numerically observable patterns, we use the totally unscaled system (1.1) with $c = 0$, where $'$ denotes differentiation with respect to the spatial variable x appearing in the original PDE (1.1). The only exception is that we set $A = \delta^2 a$, as we showed was necessary in section 2.

First, we note that the leading order of the period of Γ_P is determined by the time Γ_P spends near $\mathcal{M}$, specifically exponentially close to a hyperbolic orbit Γ_C (4.7) on $\mathcal{M}$. Second, we observe that the exact position of the take-off and touch-down points $(u_P, \mp p_P)$ has no leading order influence on the period of Γ_P. Hence, the period is determined by the time it takes Γ_C to travel from $u = 0$, $p > 0$ to $u = 0$, $p < 0$ via the symmetry point $(U_{\max}, 0)$. Here, we have to be aware that we do not get confused by the notation: the $(u, p, v, q) = (\hat{u}, \hat{p}, \hat{v}, \hat{q})$ in (2.9) are rescaled versions of the 'original' (u, p, v, q) in (1.2). By (2.4) we see that $\hat{u} = \delta^\alpha u$. Thus, the jump of Γ_P occurs $\mathcal{O}(\delta^\alpha)$ close to $\{u = 0\}$, and neglecting this $\mathcal{O}(\delta^\alpha)$ error has no leading order influence as long as we consider $\alpha > 0$. Furthermore, we note by (4.8) that the introduction of $U_{\max}$ coincided with scaling the $\hat{u}$ of (2.5) back to the original u, since $\varepsilon^3 = \delta$ if $\alpha = 1$, see (2.8). This is also the case for a general choice of α.

It is easy to check that the u-coordinate of $\Gamma_C(x)$ is given by

$$u_C(x) = 1 - (1 - U_{\max}) \cosh(\delta\sqrt{a}x).$$

Thus, $u_C(x) = 0$ for $x = x_C$ such that $\cosh(\delta\sqrt{a}x_C) = 1/(1 - U_{\max})$. This equation can be solved, and by the symmetry (4.1) we conclude that the period, or the length, $\mathcal{T}_P$ of Γ_P is

given to leading order by:

$$\mathcal{T}_P = \mathcal{T}_P(U_{\max}) = \frac{2}{\delta\sqrt{a}} \log\left(\frac{1+\sqrt{2U_{\max}-U_{\max}^2}}{1-U_{\max}}\right). \tag{4.10}$$

Equivalently, one can express $U_{\max}$ in terms of $\mathcal{T}_{\mathcal{P}}$. If we define the quantity E by

$$E = \mathrm{e}^{\frac{1}{2}\mathcal{T}_{\mathcal{P}}\delta\sqrt{a}}$$

then we can use (4.10) to find an explicit expression for $U_{\max}$:

$$U_{\max} = \frac{(E-1)^2}{E^2+1}(+\text{h.o.t.}) \tag{4.11}$$

which is less than 1. Note that we did not need an assumption on the value of α in order to determine this $U_{\max}$, this is clear since the period $\mathcal{T}_P$ (4.10) is independent of α to leading order. It is also possible to determine an approximation for the maximum value $V_{\max}$ of V, the second component of equation (1.1), at the peak of the pulse: $V_{\max}$ is determined by the value of $u_P = \hat{u}_P$ (4.9) during the jump through the fast field. In the scaled coordinates, $V_{\max}$ is determined to leading order by the maximal value of v of an unperturbed homoclinic orbit (3.3) at $u_0 = u_P$: $v_{\max} = 3b/2u_P$. By scaling backwards using (2.4), we find:

$$V_{\max} = \frac{\sqrt{a(2U_{\max}-U_{\max}^2)}}{2\delta^{\frac{1}{3}\alpha}\sqrt{b}}$$

to leading order. By (2.4) we see that $\delta^{\alpha/3}\sqrt{b} = \sqrt{B}$, thus we did not need to know the explicit value of α to compute $V_{\max}$: it can be avoided by scaling b back to B. The same is also true for the explicit value of $U_{\min}$, the minimal value of u during a period: $U_{\min}$ is a rescaled version of u_P, (4.9), which does not depend explicitly on α if we reintroduce B by (2.4). Thus, to leading order we find:

$$V_{\max} = \frac{\sqrt{a(2U_{\max}-U_{\max}^2)}}{2\sqrt{B}} \qquad U_{\min} = \frac{3B\sqrt{B}}{\sqrt{a(2U_{\max}-U_{\max}^2)}}. \tag{4.12}$$

Note that in the limit $U_{\max} \uparrow 1$ these expressions tend to the values $V_{\max}$ and $U_{\min}$ of the one-circuit homoclinic orbit described by theorem 4.1:

$$V_{\max} = \frac{1}{2}\sqrt{\frac{a}{B}} \qquad U_{\min} = 3B\sqrt{\frac{B}{a}}. \tag{4.13}$$

4.3. The special case $\alpha = 0$

Here we focus on the, in a certain sense, degenerate case $\alpha = 0$ (and we still assume $\gamma = c = 0$). When $\alpha = 0$, the scalings (2.4) imply that both (2.5) and (2.9) reduce to the unscaled system (1.4) with $A = \delta^2 a = \varepsilon^2 a$. Note that the numerical simulations suggested introducing the parameter $\alpha > 0$; the minimum value of u and the maximum value of v during a 'pulse excursion' scale with some power of δ (see section 2 and the simulations in section 6). Therefore, the choice $\alpha = 0$ does not seem to correspond to numerically stable patterns. However, from the point of view of the phase space analysis of sections 4.1 and 4.2, it is an important limit case at which interesting bifurcations occur.

One of the main differences between the cases $\alpha = 0$ and $\alpha > 0$ is the fact that the approximation of (3.6) by (3.7) is no longer valid as remarked at the end of section 3.1; (3.7) needs to be replaced by

$$\ell^{U,S}: \qquad p = \mp\varepsilon\sqrt{a}(1-u) \tag{4.14}$$

where we still write ε instead of δ. More generally, we note that the hyperbolic solutions Γ_C of the slow flow on $\mathcal{M}$ are now given by

$$p^2 = \varepsilon^2 a[(1-u)^2 - (1-U_{\max})^2] \qquad U_{\max} \leqslant 1 \tag{4.15}$$

instead of (4.7) (see figure 3(*b*)). Since the expressions for T_o and T_d still remain as in (3.21), with b replaced by the unscaled B (of $\mathcal{O}(1)$), we see that it is possible to have either zero, one or two intersections of T_o with ℓ^U or Γ_C, instead of always just one as is the case if $\alpha > 0$. The u-coordinate of $\Gamma_C \cap T_o$ is to leading order a solution of

$$F(u; U_{\max}) \stackrel{\text{def}}{=} u^2[(1-u)^2 - (1-U_{\max})^2] = \frac{9B^3}{a} \qquad u \leqslant U_{\max} \tag{4.16}$$

by (3.21) and (4.15). The function $F(u; U_{\max})$ is positive for $u \in (0, U_{\max})$ and has a maximum at $u_+ = u_+(U_{\max})$; u_+ increases monotonically as a function of $U_{\max}$; $u_+(0) = 0$, $u_+(1) = \frac{1}{2}$. The maximal value of $F(u, U_{\max})$ in the interval $[0, U_{\max}]$, $F_+(U_{\max}) = F(u_+(U_{\max}), U_{\max}))$ also increases monotonically as function of $U_{\max}$:

$$F_+(U_{\max}) \leqslant F(\tfrac{1}{2}, 1) = \tfrac{1}{16}.$$

As a consequence, we find that (4.16) has no solutions if

$$\frac{9B^3}{a} \geqslant \frac{1}{16} \qquad \text{or} \qquad a \leqslant 144B^3$$

to leading order. If $a \geqslant 144B^3$, then (4.16) has two distinct solutions for $U_{\max}$ not too small. Note that $F_+(U_{\max}) \downarrow F(0,0) = 0$ as $U_{\max} \downarrow 0$, thus, for any pair (a, b) such that $a \geqslant 144B^3$ there exists a critical $U_{SN} = U_{SN}(a, B)$ such that (4.15) has two solutions for $U_{\max} > U_{SN}$ and no solutions for $U_{\max} < U_{SN}$ (in this interpretation we have $U_{SN}(a, B) = 1$ if $a = 144B^3$).

The intersections $\Gamma_C \cap T_o$ all correspond to periodic orbits of the type described by theorem 4.2 (the argument is exactly the same as that in the proof of theorem 4.2). The orbit Γ_C merges with $\ell^U \cup \ell^S$ (3.6) for $U_{\max} = 1$, thus, the intersections $\Gamma_C \cap T_o$ then correspond to orbits homoclinic to saddle point S, as described in theorem 4.1. Combinations of orbits from both intersections can also be constructed to create more complicated periodic orbits. We can summarize the above in the following.

Theorem 4.3. *For every ε sufficiently small, $\alpha = 0$, $a \geqslant 144B^3 + \mathcal{O}(\varepsilon)$ and for any $U_{SN}(a, B) < U_{\max} < 1$, the system (2.9) with $\gamma = 0$ has two distinct slow/fast periodic orbits. These orbits merge in a saddle node bifurcation as $U_{\max} \downarrow U_{SN}$. The periodic orbits become two distinct orbits homoclinic to the saddle S as $U_{\max} \uparrow 1$. The bifurcation curve $a = 144B^3 + \mathcal{O}(\varepsilon)$ corresponds to $U_{SN}(a, B) = U_{\max} = 1$: here a saddle node bifurcation of homoclinic orbits takes place. Finally, when $\alpha = 0$, there are no periodic or homoclinic orbits for $a \leqslant 144B^3 + \mathcal{O}(\varepsilon)$.*

Finally, we make a short remark on the transition from $\alpha = 0$ to $\alpha \neq 0$. Theorem 4.3 seems to contradict theorems 4.1 and 4.2 since somewhere between $\alpha = 0$ and $\alpha \neq 0$ periodic/homoclinic orbits are either created or annihilated. Here, we only consider the homoclinic orbits and show that a contradiction does not exist. The argument for the periodic orbits is essentially the same but computationally more cumbersome. We once more write down ℓ^U for $\alpha \neq 0$ (see (3.6) and (3.5) with $\gamma = 0$):

$$\ell^U: \qquad p = -\varepsilon\sqrt{a}(1 - \varepsilon^{\frac{3}{2}(\rho-1)}u).$$

This formula reduces to (4.14) as $\alpha \downarrow 0$ (i.e. $\rho \downarrow 1$). Using the full expression for ℓ^U, the intersection $\ell^U \cap T_o$ is determined to leading order by

$$u(1 - \varepsilon^{\frac{3}{2}(\rho-1)}u) = 3b\sqrt{\frac{b}{a}}.$$

Thus, there is only one $\mathcal{O}(1)$ solution if *'ε is sufficiently small'*. However, if $\alpha \downarrow 0$ then $\varepsilon^{\frac{3}{2}(\rho-1)} \uparrow 1$ and there can be none or two solutions. Thus, a possible contradiction between theorems 4.1 and 4.3 is avoided by employing the 'traditional phrase' *'ε is sufficiently small'*. Theorem .1 holds for $\varepsilon < \varepsilon_0 = \varepsilon_0(\alpha)$, since ε_0 must become 'very small' if α becomes small, i.e. since $\lim_{\alpha \downarrow 0} \varepsilon_0(\alpha) = 0$, see also remark 2.2.

5. Travelling patterns

In this section, we search analytically for solutions of (1.1) that travel with a constant speed c and which do not change shape in a comoving coordinate system. Note that the self-replicating pulse solutions (numerically) found in [22] are not of this type. It was deduced in section 2 that c should be at least $\mathcal{O}(\delta^{(1+\beta)})$ for some $\beta \geqslant 2 - \alpha > \frac{1}{2}$, where α measures the magnitude of $u = \delta^\alpha \hat{u}$, the u-coordinate of a homoclinic solution to $S \in \mathcal{M}$ of the unscaled system (1.2) or (1.4), during an excursion through the fast field. In other words, α measures the magnitude of the minimal value of the solution $U(x, t)$ of the PDE (1.1) in the region where $V(x, t)$ is peaked, that is, $V(x, t)$ is not exponentially close to 0.

The main result (theorem 5.1) of this section is that for $0 \leqslant \alpha < \frac{3}{2}$ there cannot exist orbits homoclinic to S in (2.9) for $c \neq 0$. Thus, theorem 5.1 implies that the one-parameter (c) family of 'dissipative perturbations' of the symmetric system (1.4) with $c = 0$ destroys the entire three-parameter family (a, b, α) of orbits homoclinic to S. There are no travelling solitary pulse solutions to the PDE (1.1).

This result is surprising in the context of the geometric singular perturbation analysis of sections 2–4. First, by simple counting arguments alone, one should expect large families of orbits homoclinic to S. Both the stable and unstable manifolds of S are two-dimensional, the phase space is four-dimensional, and there are three free parameters in (1.4), or, by the scalings, even five—$a, b, \gamma, \sigma, \rho$—in (2.9). Second, homoclinic orbits are known to persist in a wide variety of systems subject to small-amplitude perturbations. For $\gamma = 0$, theorem 4.1 states that for any $a > 0$, $b > 0$ and $0 < \alpha < \frac{3}{2}$ there is a homoclinic solution to S which corresponds to a stationary pulse solution of (1.1); moreover, when $\gamma = 0$ and $\alpha = 0$, theorem 4.3 gives the existence of either two or zero orbits homoclinic to S, depending on the parameters a and B. The fact that the unstable and stable manifolds of $\mathcal{M}$ still have a two-dimensional intersection surface while there are no parameter combinations such that the stable and unstable manifolds of $S \in \mathcal{M}$ intersect for $\gamma \neq 0$ shows that the behaviour of system (2.9) is degenerate when $\gamma = 0$.

The system's degeneracy stems in part from the fact that for travelling pulses with speed c smaller than $\mathcal{O}(\delta^{(3-\alpha)})$ (i.e. $\sigma > 0$ in (2.9)), the magnitude of the evolution of the slow field—$\mathcal{O}(\varepsilon)$—is much larger than the perturbation term in the fast field, which is of $\mathcal{O}(\varepsilon^{(2+\sigma)})$. We perform a rather subtle and detailed perturbation analysis, since there must be some kind of balance between these effects in order for homoclinic orbits to exist. Our analysis is much more delicate than that performed in section 3.

We focus on the (non-)existence of one-pulse solutions to (2.9) that are homoclinic to S. In section 3.2, we defined the take-off curve $T_o \in \mathcal{M}$. Orbits $\Gamma^-_{\mathcal{M}}(t; x_0^-) \subset \mathcal{M}$ with initial condition $x_0^- \in T_o$ determine the behaviour, for $-t \gg 0$, of all orbits $\Gamma(t; x_0)$ in the first intersection of $W^U(\mathcal{M})$ and $W^S(\mathcal{M})$ (with $x_0 \in W^U(\mathcal{M}) \cap W^S(\mathcal{M}) \cap \{q = 0, v \neq 0\}$).

Thus, an intersection $(u_0^-, p_0^-, 0, 0)$ of T_o and ℓ^U—see (3.6)—corresponds to an orbit $\Gamma(t; x_0) \in W^U(\mathcal{M}) \cap W^S(\mathcal{M})$ which 'originates' on S, i.e. $\lim_{t\to-\infty} \Gamma(t) = S$. Note that the intersection point $(u_0^-, p_0^-, 0, 0)$ determines the lower endpoint of the interval on ℓ^U for which $\Gamma(t; x_0)$ is close to ℓ^U; however, by definition, $\|\Gamma(t; x_0) - (u_0^-, p_0^-, 0, 0)\| \geqslant \mathcal{O}(\varepsilon)$ for $t = \mathcal{O}(1)$.

By construction, $\Gamma(t, x_0)$ touches down on $\mathcal{M}$ and is exponentially close (for $t \geqslant \mathcal{O}(\frac{1}{\varepsilon})$) to an orbit $\Gamma^+_{\mathcal{M}}(t; x_0^+)$ with $x_0^+ \in T_d$. Thus, Γ_h is a (one-circuit) homoclinic solution to S if $x_0^+ = (u_0^+, p_0^+, 0, 0) \in \ell^S \cap T_d$. Let $x_0 = (u_0, p_0, v_0, 0) \in \{\Delta K = 0\}$, see (3.15). The corresponding $x_0^\pm = (u_0^\pm, p_0^\pm, 0, 0)$ are given by the expressions (3.21) for T_o and T_d. To construct $\Gamma_h(t; x_0)$, we have to impose that $(u_0^-, p_0^-) \in T_o \cap \ell^U$ and $(u_0^+, p_0^+) \in T_d \cap \ell^S$:

$$\begin{cases} -\varepsilon\sqrt{a} + \text{h.o.t.} = \dfrac{1}{2}\varepsilon\left(\varepsilon^\sigma \gamma u_0 - \dfrac{6b\sqrt{b}}{u_0}\right) + \text{h.o.t.} \\ +\varepsilon\sqrt{a} + \text{h.o.t.} = \dfrac{1}{2}\varepsilon\left(\varepsilon^\sigma \gamma u_0 + \dfrac{6b\sqrt{b}}{u_0}\right) + \text{h.o.t.} \end{cases} \tag{5.1}$$

Adding and subtracting these two equations, we find

$$\varepsilon^\sigma \gamma u_0 = \text{h.o.t.} \qquad \text{and} \qquad 2\sqrt{a} = \frac{6b\sqrt{b}}{u_0} + \text{h.o.t.} \tag{5.2}$$

Thus, we recover (4.2). Moreover, we conclude that $\sigma > 0$, since neither γ nor u_0 can be smaller than $\mathcal{O}(1)$ by the scalings of section 2, and since we assumed that $\gamma \neq 0$, otherwise we merely recover the stationary pulse solutions constructed in section 4.

However, so far it is not clear at all that the term $\varepsilon^\sigma \gamma u_0$ cannot be 'balanced' by one of the higher-order terms in (5.1). In fact, *a priori*, one expects that the computation of the higher-order terms in (5.1) will lead to equations for σ and γ. Given the fact that a travelling wave exists if a solution of system (5.1) can be found, but does not if no solution exists, we now proceed to find the higher-order terms using the same method as we employed above. We find the curve on $W^S(\mathcal{M}) \cap W^U(\mathcal{M}) \cap \{q = 0\}$ along which $\Delta K = 0$ up to and including as many higher-order terms as necessary. Then, we derive expressions for T_o and $T_d \subset \mathcal{M}$ and determine the intersections $T_o \cap \ell^U$ and $T_d \cap \ell^S$, again obtaining as many higher-order terms as are necessary. To achieve both of these objectives, we have to extend the expansion (3.11) so that we can compute a more accurate approximation of an orbit $\Gamma(t; x_0) = (u(t; x_0), p(t; x_0), v(t; x_0), q(t; x_0))$ with initial condition $x_0 \in W^S(\mathcal{M}) \cap W^U(\mathcal{M}) \cap \{q = 0\}$. Only then can we determine with sufficient precision the initial conditions $x_0^\pm$ of the orbits $\Gamma^\pm_{\mathcal{M}}(t; x_0^\pm)$, which determine T_o and T_d as defined by (3.20).

As we already did in section 3, we will frequently exploit the fact that many terms, especially those of lower order, in the expansion of the solutions $\Gamma(t) = (u(t), p(t), v(t), q(t))$ are either odd or even. This simple observation forms the foundation of the non-existence proof below. This special character of the lower-order terms in the expansion of $\Gamma(t)$ can be interpreted as the remains of the symmetry (4.1) which exists in the case $\gamma = 0$: all solutions $\Gamma(t) = (u(t), p(t), v(t), q(t)) \subset W^U(\mathcal{M}) \cap W^S(\mathcal{M})$ with $\Gamma(0) \in \{q = 0\}$ must have $p(0) = 0$, which yields, by the symmetry (4.1): $u(t)$ and $v(t)$ are even, $p(t)$ and $q(t)$ are odd. Since the non-symmetric dissipative effects are of order $\mathcal{O}(\varepsilon^{(2+\sigma)})$ or higher, it is clear that the lower-order terms in the expansions of $u(t)$ and $v(t)$ must be even as function of t, while those of $p(t)$ and $q(t)$ must be odd. Before we present the details of the analysis, we state the main result.

Theorem 5.1. *For $\gamma \neq 0$, $0 \leqslant \alpha < \frac{3}{2}$, and $0 < \delta \ll 1$, there are no one-pulse solutions homoclinic to S in equation (1.4) (equivalently (2.5) or (2.9)).*

Remark 5.1. For $\sigma = 0$ the result of this theorem follows immediately from the straightforward application of the ideas developed in section 3 that led to (5.2). The case of $\sigma = 0$ (i.e. $\beta = 2 - \alpha$) is the significant degeneration, recall (2.5); see [5] for a discussion of what constitutes significant degeneration in singularly perturbed systems. By contrast, we shall see in the numerical simulations of section 6 that the self-replicating pulses do travel with this critical speed $c = \mathcal{O}(\delta^{(1+\beta)}) = \mathcal{O}(\delta^{(3-\alpha)})$.

Proof of theorem 5.1. For simplicity we first consider the case $0 < \sigma < 1$ and $\rho > 1 + \frac{2}{3}\sigma$ so that $\dot{p} = \varepsilon u v^2 +$ terms smaller than $\mathcal{O}(\varepsilon^{3+\sigma})$ (recall $\rho = 3$ when $\alpha = 1$). These conditions will minimize the technical difficulties, since we do not have to pay attention to the higher-order terms in the equation for $\dot{p}$. At the end, we show that the proof is readily generalized to the cases of $\sigma \geqslant 1$ and $0 < \rho \leqslant 1 + \frac{2}{3}\sigma$.

We begin by rewriting the main equations (2.9) so that we may more easily refer to them:

$$\begin{aligned} \dot{u} &= \varepsilon p \\ \dot{p} &= \varepsilon[u v^2 - \varepsilon^{\frac{1}{2}(3\rho+1)} a - \varepsilon^{(2\rho+1+\sigma)} \gamma p + \varepsilon^{(3\rho-1)} a u] \\ \dot{v} &= q \\ \dot{q} &= -u v^2 + b v - \varepsilon^{(2+\sigma)} \gamma q. \end{aligned} \tag{5.3}$$

From (3.15), we find that an orbit $\Gamma(t) = (u(t), p(t), v(t), q(t)) \in W^S(\mathcal{M}) \cap W^U(\mathcal{M})$, with $\Gamma(0) \in \{q = 0\}$, must have $p(0) = \frac{1}{2}\varepsilon^{(1+\sigma)} \gamma u(0)$ (to leading order). Thus, we need to adapt and extend (3.11) to:

$$\begin{aligned} u(t) &= u_0 + \varepsilon u_1(t) + \varepsilon^2 u_2(t) + \varepsilon^{(2+\sigma)} u_{2+\sigma}(t) + \varepsilon^3 u_3(t) + \mathcal{O}(\varepsilon^4) \\ p(t) &= \varepsilon p_1(t) + \varepsilon^{(1+\sigma)} p_{1+\sigma}(t) + \varepsilon^2 p_2(t) + \varepsilon^3 p_3(t) + \varepsilon^{(3+\sigma)} p_{3+\sigma}(t) + \mathcal{O}(\varepsilon^4) \\ v(t) &= v_0(t; u_0) + \varepsilon v_1(t) + \varepsilon^2 v_2(t) + \varepsilon^{(2+\sigma)} v_{2+\sigma}(t) + \mathcal{O}(\varepsilon^3) \\ q(t) &= q_0(t; u_0) + \varepsilon q_1(t) + \varepsilon^2 q_2(t) + \varepsilon^{(2+\sigma)} q_{2+\sigma}(t) + \mathcal{O}(\varepsilon^3). \end{aligned} \tag{5.4}$$

Remark 5.2. In writing (5.4) above, we have used some foreknowledge of the equations at each order: we did not write down those terms—such as $\epsilon^{2+\sigma} p_{2+\sigma}(t)$ and $\epsilon^{3+\sigma} u_{3+\sigma}(t)$—for which it is clear without much extra analysis that they are identically zero since they need to satisfy a trivial equation after the expansions are substituted into (2.9).

Here $p_{1+\sigma}(t) \equiv \frac{1}{2}\gamma u_0$ by (3.15), since $\dot{p}_{1+\sigma} = 0$. We may assume, as in section 3, that $u(0) = u_0$ and all higher-order terms of u are 0 at $t = 0$. In this fashion, u_0 again parametrizes the curve $W^S(\mathcal{M}) \cap W^U(S) \cap \{q = 0\}$; $p(0)$ and $v(0)$ are determined as functions of u_0 up to any order in ε. This yields that $u_{2+\sigma}(t) = \frac{1}{2}\gamma u_0 t$. Also after inserting (5.4) into (5.3), we immediately find that

$$u_1 \equiv 0 \qquad p_1 \text{ odd} \qquad u_2 \text{ even} \qquad p_{1+\sigma} = \tfrac{1}{2}\gamma u_0 \qquad v_1 \equiv 0 \qquad q_1 \equiv 0 \tag{5.5}$$

see also section 3.

The following simple result helps us to establish the parity (odd/even) properties of further terms in the expansion of v.

Lemma 5.2. *Let $f(t)$ and $g(t)$ be real-analytic functions. Let $z(t)$ be a solution of*

$$\ddot{z} + f(t) z = g(t) \qquad \text{with } z(0) = z_0,\ \dot{z}(0) = 0.$$

Then $z(t)$ is an even function of t if both f and g are even and $z(t)$ is odd if g is odd and $z_0 = 0$.

This lemma is proven by computing the derivatives $\mathrm{d}^n z/\mathrm{d}t^n$ inductively and then evaluating them at $t = 0$. Applying this lemma to

$$\ddot{v}_2 + (2u_0v_0 - b)v_2 = -u_2v_0^2 \tag{5.6}$$

we see that v_2 is also even (and q_2 odd). Note that it is possible to obtain an explicit expression for v_2. The second-order differential operator consists of a soliton potential created by the unperturbed homoclinic solution $v_0(t)$ with solutions given by associated Legendre polynomials, see for example problem 5, section 23 of [15]. However, we will not use this.

Next, we need to extract more information from the condition that $\Gamma = (u, p, v, q)$ lies in $W^S(\mathcal{M}) \cap W^U(\mathcal{M})$ in order to determine the initial conditions on $v_2(t)$, $p_2(t)$, etc. In other words, we have to impose that $\Delta K = 0$ on Γ, which using (5.5), amounts to:

$$\begin{aligned}\Delta K(u_0, p_0) = {} & \varepsilon^2 \int_{-\infty}^{\infty} \tfrac{1}{3} p_1 v_0^3 \,\mathrm{d}t + \varepsilon^{(2+\sigma)} \int_{-\infty}^{\infty} (\tfrac{1}{3} p_{1+\sigma} v_0^3 - \gamma q_0^2) \,\mathrm{d}t \\ & + \varepsilon^3 \int_{-\infty}^{\infty} \tfrac{1}{3} p_2 v_0^3 \,\mathrm{d}t + \varepsilon^4 \int_{-\infty}^{\infty} (\tfrac{1}{3} p_3 v_0^3 + p_1 v_0^2 v_2) \,\mathrm{d}t \\ & + \varepsilon^{(4+\sigma)} \int_{-\infty}^{\infty} (\tfrac{1}{3} p_{3+\sigma} v_0^3 + p_1 v_0^2 v_{2+\sigma} + p_{1+\sigma} v_0^2 v_2 - 2\gamma q_0 q_2) \,\mathrm{d}t + \mathcal{O}(\varepsilon^5).\end{aligned} \tag{5.7}$$

The first integral vanishes, since $p_1(t)$ is odd and $v_0(t)$ is even. Thus, by imposing $\Delta K = 0$ we recover $p_{1+\sigma} = \frac{1}{2}\gamma u_0$ (see (3.15)). Next, the initial value $v_2(0)$ is determined by the value of $K|_\Gamma$ at $q = 0$. We see from the first term in (5.7) that $v_2(0) \neq 0$, since $p_1(t)$ is odd and $\int_{-\infty}^{0} \frac{1}{3} p_1 v_0^3 \,\mathrm{d}t \neq 0$. Hence, $K|_\Gamma \cap \{q = 0\} = \mathcal{O}(\varepsilon^2)$.

We now determine $v_{2+\sigma}(t)$ and its initial value. Since the terms in the integrand of the $\mathcal{O}(\varepsilon^{(2+\sigma)})$ integral are both even, we conclude that also the accumulated change at the $\mathcal{O}(\varepsilon^{(2+\sigma)})$ level in K along a solution Γ over the time intervals $(-\infty, 0)$ and $(0, \infty)$ are the same. In fact, the two semi-infinite integrals are equal and each is precisely half of the full integral. But, the full integral must be identically zero along a persistent homoclinic solution, Γ. So, each of the half integrals is zero, as well. Hence, unlike v_2, $v_{2+\sigma}$ does not have to 'correct' the value of K at $t = 0$, and we have $v_{2+\sigma}(0) = 0$. Also, using (5.5), the equation for $v_{2+\sigma}$ reads

$$\ddot{v}_{2+\sigma} + (2u_0v_0 - b)v_{2+\sigma} = -\gamma(q_0 + \tfrac{1}{2}u_0v_0^2 t).$$

Therefore, we conclude, by lemma 5.2, that $v_{2+\sigma}$ is an odd function of time.

Higher-order terms in the expansion of $p(t)$ along Γ are obtained as follows. By straightforward calculations similar to that for $p_1(t)$, we find that $p_2(t) \equiv p_2(0)$ and $p_3(t) = p_3(0)+$ an odd function. But, from the $\mathcal{O}(\varepsilon^3)$ and $\mathcal{O}(\varepsilon^4)$ levels of (5.7), we know that $p_2(0) = p_3(0) = 0$, since ΔK must be 0. Next, the equation for $p_{3+\sigma}$ reads:

$$\dot{p}_{3+\sigma} = u_{2+\sigma}v_0^2 + 2u_0v_0v_{2+\sigma}.$$

Here, we have used $\rho > 1 + \frac{2}{3}\sigma$. Thus, $p_{3+\sigma}(t)$ is even, because $u_{2+\sigma}(t)$ and $v_{2+\sigma}(t)$ are odd.

What do the above terms tell us about ΔK and $p(0)$? They imply that all terms in the integral at the $\mathcal{O}(\varepsilon^{(4+\sigma)})$ level of (5.7) are even. Hence, the requirement $\Delta K = 0$ fixes $p_{3+\sigma}(0)$ as a function of u_0 and γ: $p_{3+\sigma}(0) = F(u_0; \gamma)$. Of course, $F(u_0; \gamma)$ can be computed explicitly, but this is not needed here. Therefore, the curve $\{\Delta K\} = 0 \subset W^S(\mathcal{M}) \cap W^U(\mathcal{M}) \cap \{q = 0\}$ is given by

$$p(0) = \varepsilon^{(1+\sigma)} p_{1+\sigma}(0) + \varepsilon^{(3+\sigma)} p_{3+\sigma}(0) = \tfrac{1}{2}\varepsilon^{(1+\sigma)}\gamma u_0 + \varepsilon^{(3+\sigma)} F(u_0; \gamma) + \mathcal{O}(\varepsilon^4). \tag{5.8}$$

This completes the first part of the proof.

In this second part of the proof, we construct T_o and T_d to sufficiently high order. For a given $x_0 = (u_0, p(0), v(0), 0) \in W^S(\mathcal{M}) \cap W^U(\mathcal{M})$, we must find $x_0^\pm = (u_0^\pm, p_0^\pm, 0, 0) \in \mathcal{M}$ such that the orbits $\Gamma_\mathcal{M}(t; x_0^\pm)$ are exponentially close to $\Gamma(t; x_0)$ for $\pm t \geqslant \mathcal{O}(\frac{1}{\varepsilon})$. First, we write expansions for $\Gamma_\mathcal{M}(t; x_0^\pm)$ similar to the expansion above for $\Gamma(t; x_0)$. By (5.3), we see that $\dot{p} = o(\varepsilon^{(3+\sigma)}) \ll \mathcal{O}(\varepsilon^{(3+\sigma)})$ on $\mathcal{M}$ (since $\rho > 1 + \frac{2}{3}\sigma$), which yields, for $t = \mathcal{O}(1)$:

$$\begin{cases} p^\pm(t) = p_0^\pm + o(\varepsilon^{(3+\sigma)}) \\ u^\pm(t) = u_0^\pm + \varepsilon p_0^\pm t + o(\varepsilon^{(4+\sigma)}). \end{cases} \tag{5.9}$$

Second, we find $p_0^\pm$ and $u_0^\pm$ using the functions $p_j(t)$ computed above in the expansion of $p(t)$ along $\Gamma(t)$. Let the functions $G_j(u_0)$ and $P_j(t; u_0)$ $(j = 1, 3, 3+\sigma)$ be defined by:

$$p_j(t; u_0) = G_j(u_0) + P_j(t; u_0) \qquad \text{with } \lim_{t\to\infty} P_j(t; u_0) = 0 \qquad (j = 1, 3).$$

By construction,

$$G_1(u_0) = \frac{1}{2}\Delta p(u_0) = \frac{3b\sqrt{b}}{u_0} \tag{5.10}$$

where we recall (3.12) and (3.18). In terms of these functions, we may write the expansion of $p(t)$ for $t > 0$ as

$$\begin{aligned} p(t) = {} & (\varepsilon G_1 + \varepsilon^{(1+\sigma)} p_{1+\sigma}(0) + \varepsilon^3 G_3 + \varepsilon^{(3+\sigma)}(p_{3+\sigma}(0) + G_{3+\sigma})) \\ & + (\varepsilon P_1(t) + \varepsilon^3 P_3(t) + \varepsilon^{(3+\sigma)} P_{3+\sigma}(t)) \end{aligned}$$

where we have neglected higher-order terms. Also, for $t > 0$, the expansion of $u(t)$ along a homoclinic orbit $u(t)$ is known from $p(t)$ and (5.3). Now, the initial condition $p_0^+ = p_0^+(u_0)$ is determined by the condition that $p^+(t)$ and $p(t)$ have the same asymptotic behaviour. Since the $P_j(t)$'s vanish for large t, we conclude from (5.9) that

$$p_0^+(u_0) = \varepsilon G_1(u_0) + \varepsilon^{(1+\sigma)} p_{1+\sigma}(0) + \varepsilon^3 G_3(u_0) + \varepsilon^{(3+\sigma)}(p_{3+\sigma}(0) + G_{3+\sigma}(u_0)) + \text{h.o.t.} \tag{5.11}$$

Also, by defining

$$H_1(u_0) = \int_0^\infty P_1(t; u_0)\, \mathrm{d}t$$

we find by (5.3) and (5.9) that

$$u_0^+(u_0) = u_0 + \varepsilon^2 H_1(u_0) + \mathcal{O}(\varepsilon^4). \tag{5.12}$$

The p_0^+ and u_0^+ coordinates of T_o are clearly implicitly related, since both are functions of u_0 by (5.8). Taylor expanding the functions G_j in the right-hand side of (5.11) about u_0^+ and using (5.12), we get:

$$\begin{aligned} p_0^+(u_0) = {} & \varepsilon G_1(u_0^+) + \varepsilon^{(1+\sigma)} p_{1+\sigma}(0) + \varepsilon^3 (G_3(u_0^+) - G_1'(u_0^+) H_1(u_0^+)) \\ & + \varepsilon^{(3+\sigma)}(p_{3+\sigma}(0) + G_{3+\sigma}(u_0^+)) + \text{h.o.t.} \end{aligned} \tag{5.13}$$

Similarly, one must Taylor expand the functions F and

$$p_{1+\sigma}(0) = \frac{\gamma}{2} u_0 = \frac{\gamma}{2}(u_0^+ - \varepsilon^2 H_1(u_0^+)) + \text{h.o.t.}$$

Therefore, we find

$$\begin{aligned} T_d: \qquad & p - \varepsilon G_1 - \varepsilon^3 (G_3 - G_1' H_1) - \varepsilon^{(3+\sigma)} G_{3+\sigma} = \tfrac{1}{2}\varepsilon^{(1+\sigma)} \gamma u \\ & + \varepsilon^{(3+\sigma)}(F - \tfrac{1}{2}\gamma H_1) + \text{h.o.t.} \end{aligned} \tag{5.14}$$

where $p = p_0^+$, $u = u_0^+$ and $G_1' = \mathrm{d}G_1/\mathrm{d}u(u)$.

Using the parity (odd/even) properties of the functions $p_j(t)$, we immediately find the analogous results for p_0^-, u_0^- and T_o:

$$\begin{aligned} p_0^-(u_0) &= -\varepsilon G_1(u_0) - \varepsilon^{(1+\sigma)} p_{1+\sigma}(0) - \varepsilon^3 G_3(u_0) + \varepsilon^{(3+\sigma)}(p_{3+\sigma}(0) \\ &\quad + G_{3+\sigma}(u_0)) + \text{h.o.t.} \\ u_0^-(u_0) &= u_0 + \varepsilon^2 H_1(u_0) + \mathcal{O}(\varepsilon^4). \end{aligned} \tag{5.15}$$

The u_0^- and p_0^- coordinates for T_o are also implicitly related, since both are functions of u_0 by (5.8). This relation can be made explicit in a straightforward manner:

$$\begin{aligned} T_\mathrm{o}: \qquad & p + \varepsilon G_1 + \varepsilon^3(G_3 - G_1' H_1) - \varepsilon^{(3+\sigma)} G_{3+\sigma} = \tfrac{1}{2}\varepsilon^{(1+\sigma)}\gamma u \\ & + \varepsilon^{(3+\sigma)}(F - \tfrac{1}{2}\gamma H_1) + \text{h.o.t.} \end{aligned} \tag{5.16}$$

where $p = p_0^-$, $u = u_0^-$ and $G_1' = \mathrm{d}G_1/\mathrm{d}u(u)$. Note that to leading order, these expressions (5.14) and (5.16) correspond to those obtained for T_o and T_d in (3.21).

A travelling pulse with a speed $c = \delta^{(1+\beta)}\gamma$, such that $\beta > 2 - \alpha$, or equivalently $\sigma > 0$, exists for u_0 such that the corresponding orbit $\Gamma_h(t; x_0)$, with initial condition $x_0 = (u_0, p(0; u_0), v(0; u_0), 0)$, lies in the intersection of $W^S(S)$ and $W^U(S)$. In other words, the take-off point $(u_0^-(u_0), p_0^-(u_0))$ of Γ_h must be on $\ell^U = W^U(S) \cap \mathcal{M}$, and the touch-down point $(u_0^+(u_0), p_0^+(u_0)) \in \ell^S$. Thus, we have to compute the intersections $T_\mathrm{o} \cap \ell^U$ and $T_\mathrm{d} \cap \ell^S$. Expanding (3.6) yields:

$$\ell^U: \qquad p = -\varepsilon\sqrt{a} + \varepsilon^{\frac{1}{2}(3\rho-1)}\sqrt{a}u + \text{h.o.t.}$$

where the higher-order terms are smaller than $\mathcal{O}(\varepsilon^{(3+\sigma)})$ for any $\sigma > 0$. A similar expression can be obtained for ℓ^S. The homoclinic solution Γ_h exists for u_0, γ and σ which satisfy the system of equations given by $T_\mathrm{o} \cap \ell^U$ and $T_\mathrm{d} \cap \ell^S$, where u_0 appears only implicitly in the equations through $u = u_0^\pm(u_0)$ in the expressions (5.16) for T_o and (5.14) for T_d. However, we observe by (5.12) and (5.15) that $u_0^-(u_0) = u_0^+(u_0)$ up to $\mathcal{O}(\varepsilon^4)$, thus we can solve the system defined by $T_\mathrm{o} \cap \ell^U$ and $T_\mathrm{d} \cap \ell^S$ in terms of $u = u_0^- = u_0^+$ and γ, instead of u_0 and γ. Adding these two equations, and dividing by $\varepsilon^{(1+\sigma)}$, yields:

$$\gamma u + \varepsilon^2(2G_{3+\sigma} - \gamma H_1 + 2F) = \text{h.o.t.} \tag{5.17}$$

We now observe that it is not possible to solve this equation unless we admit $\gamma = 0$: due to the symmetries there are no terms left which can 'balance' the $\mathcal{O}(1)$ term γu. Note that $u \neq 0$ by (5.2). This proves the theorem in the case $0 < \sigma < 1$, $\rho > 1 + \frac{2}{3}\sigma$.

Before we go on with the proof of the general case, we make two observations. First, we note that subtracting the equations for $T_\mathrm{o} \cap \ell^U$ and $T_\mathrm{d} \cap \ell^S$ just gives higher-order corrections to the critical value of u_0 (see (5.2)). Second, we note that *a priori* one might think that the $\mathcal{O}(\varepsilon^2)$ part of (5.17) causes problems, since it also must be zero. However, one can check, in a straightforward manner, the behaviour of the terms in (5.4) as function of γ and conclude that $G_{3+\sigma} = G_{3+\sigma}(u_0; \gamma) = \gamma\hat{G}_{3+\sigma}$ and $F = F(u_0; \gamma) = \gamma\hat{F}(u_0)$. Thus, the $\mathcal{O}(\varepsilon^2)$ term also disappears when $\gamma = 0$.

The question now is: what happens if ρ and σ do not satisfy these conditions? Let us first consider $1 < \sigma < 2$. It is easy to see how expansion (5.4) should be modified: the σ-dependence now only occurs at the levels $u_{2+\sigma} = u_{3+(\sigma-1)}$, $p_{1+\sigma} = p_{2+(\sigma-1)}$, $p_{3+\sigma} = p_{4+(\sigma-1)}$, $v_{2+\sigma} = v_{3+(\sigma-1)}$ and $q_{2+\sigma} = q_{3+(\sigma-1)}$. It is also easy to show that u_0, u_1, u_2, u_3 are even, v_0, v_1, v_2, v_3 are even p_1, p_2, p_3, p_4 are odd, and q_0, q_1, q_2, q_3 are odd: exactly as in the above case, these solutions do not feel the dissipative terms yet and thus obey the symmetry (4.1). The equations for $u_{2+\sigma}$, $p_{3+\sigma}$, $v_{2+\sigma}$ and $q_{2+\sigma}$ are the same as

those in the case $\sigma < 1$. Thus, the only differences between T_o, T_d in the case $0 < \sigma < 1$ and the case $1 < \sigma < 2$ are some extra *symmetrical* terms of $\mathcal{O}(\varepsilon^4)$ in (5.16) and (5.14). *These terms all cancel* when we add the equations for $T_o \cap \ell^U$ and $T_d \cap \ell^S$. Thus: *there is no change in* (5.17). Again, we have to conclude that $\gamma = 0$ and that the theorem holds.

The same will happen for any value of σ: all symmetrical contributions of the expansions will vanish when we add the equations for $T_o \cap \ell^U$ and $T_d \cap \ell^S$: (5.17) will not change, so the theorem holds. The only extra technical complications appear when $\sigma = 1, 2, \ldots$, since then we have to split the solutions $u_{2+\sigma}$, $p_{3+\sigma}$, $v_{2+\sigma}$ and $q_{2+\sigma}$ in an even and an odd part: one part takes care of the dissipative effects and the other obeys (4.1). Only the first part appears in (5.17) so that it again does not change. A similar technicality has to be taken into account in the case when ρ is less than or equal to $1 + \frac{2}{3}\sigma$: expansion (5.4) has to be adapted to include the higher-order effects in the equation for $\dot{p}$ in (5.3) which appear before the dissipative effects. However, these higher-order terms also obey symmetry (4.1), thus they will not appreciably influence (5.17). This concludes the proof of theorem 5.1. □

Remark 5.3. In section 4 we found that $\alpha = 0$ was a special case since the approximation (3.7) of (3.6) could not be used in this case. In the proof of theorem 5.1 we did not pay attention to the special case $\alpha = 0$: this is not necessary since it again has no influence on those terms in the equations for $T_o \cap \ell^U$ and $T_d \cap \ell^S$ which do not cancel after addition.

Remark 5.4. The proof of theorem 5.1 also implies the non-existence of travelling patterns consisting of the periodic stationary patterns translating uniformly in time. We recall that the central argument used to establish theorem 5.1 relies on the adiabatic Melnikov function ΔK to find solutions in the transverse intersection of the stable and unstable manifolds of $\mathcal{M}$, as well as on the calculation of Δp, to insure that the jump in the p coordinate during a fast excursion precisely bridges the gap between ℓ^U and ℓ^S. The existence of periodic patterns when $\gamma \neq 0$ relies on precisely these same two calculations. Moreover, the details are similar: the fast excursion corresponds to an orbit of the fast subsystem that lies in the transverse intersection of the slow plane's stable and unstable manifolds, and the jump in p must coincide with the horizontal distance between two points on the same hyperbolic orbit Γ_C on $\mathcal{M}$. Since these conditions have the same form as those for the travelling one-pulse solutions, arguments similar in structure to those used above show that no such solution is possible.

Remark 5.5. Besides extending to the non-existence of periodic travelling solutions, theorem 5.1 also extends to show the non-existence of N-pulse homoclinic travelling waves for any $N = \mathcal{O}(1)$, implying that the $\gamma = 0$ symmetry of (2.9) is broken and all of the orbits given by theorem 4.1 disappear when $\gamma > 0$. Instead of looking for zeroes of ΔK as we did for one-pulse orbits, however, one looks for zeroes of the appropriate inductively defined N-pulse adiabatic Melnikov function [28]: $\Delta K_N(u, p; \varepsilon) \equiv \Delta K_{N-1}(u, p; \varepsilon) + \Delta K_1(u, p + \varepsilon \frac{9b^2}{4u} \sum_{i=1}^{N-1} \tau_i)$, where τ_i denotes the period of the unperturbed periodic orbit of the fast subsystem with slow parameter u and with energy given by ΔK_{i-1}; also, $\Delta K_1(u, p) \equiv \Delta K(u, p)$, as introduced in section 3. The same proof as given in [28] for planar Hamiltonian systems depending on a slowly varying parameter (here p) implies here that ΔK_N is the correct higher-order adiabatic Melnikov function for (2.9), because the fact that $\Delta u = \mathcal{O}(\varepsilon^2)$ during each fast excursion relegates u to the status of a parameter in this calculation. Now, since the periods τ_i for $i = 1, \ldots, N-1$ only diverge logarithmically as $\varepsilon \to 0$, the arguments of the terms in the sum for ΔK_N lie close to p_0, the $p-$coordinate of the zero of ΔK. Therefore, the simple zeroes of ΔK_N lie close to those of ΔK, and the asymptotic expansions for the $N-$pulse case are similar in structure (with extra log terms

that cannot be balanced by the γ terms) to those of the one-pulse case. Thus, the same argument as used above also rules out the existence of $N-$pulse travelling waves. Note that of course one requires that $N\Delta p$ equals the horizontal distance between ℓ^U and ℓ^S, instead of requiring that Δp equal that distance.

6. Numerical simulations

In this section, we study the numerically observed dynamics of the PDE (1.1). In order to do numerical calculations, we have to restrict x to a bounded interval. However, to obtain patterns which can be described by the analysis of the previous section we only consider intervals that are long enough so that the boundaries are 'far away' and do not influence the dynamics. The simulations presented in this section have been repeated several times on intervals of different lengths. We only show the outcome of simulations on intervals which are so large that enlarging the intervals did not influence the behaviour. Moreover, we have done the simulations with different types of boundary conditions and checked that this also did not change the dynamics inside the interval.

There are three parameters in (1.1): A, B and δ. We have rescaled A and B into $A = \delta^2 a$ and $B = b\delta^{2\alpha/3}$ in section 2; α measures the magnitude of B. In this section, we focus on the choice $\alpha = 1$, this means that, as was observed in [22], we assume that $U = \mathcal{O}(\delta)$ during a 'pulse-excursion' of V. Note that this choice is not essential since we have seen in section 4.2 that the maximum and minimum values of U and V can be expressed in an unscaled form, independent of an explicit value of α, see (4.12) and (4.13). Reynolds, Pearson, Ponce-Dawson, and Hasslacher observed self-replicating pulse patterns for the choice $\delta^2 = 0.01$, $A = 0.02$ and $B = 0.079$ in (1.1) see figure 1 of [22] and figure 2 of [3]. These values correspond in our scaling to $a = 2$ and $b \approx 0.37$. Below, we shall frequently choose $\delta^2 = 0.01$, $a = 2$ and $b = 0.4$, so that we can compare with the results of [22].

6.1. The code

We used a moving-grid code to integrate system (1.1). The code, which is described in detail in [2], is designed to numerically solve systems of time-dependent PDE models in one space dimension having solutions with steep gradients in space and time. The moving-grid technique in the code is based on a Lagrangian description of the PDE model combined with a smoothed-equidistribution principle to define the grid positions at each time level. The dynamically moving adaptive grid is coupled to a discretization method which automatically discretizes the spatial part of the user-defined PDE system following the method-of-lines approach. The spatial discretization and the time-integration are carried out with a nonlinear Galerkin method and an implicit (stiff) BDF method with variable order and step-size control, respectively. It must be noted that application of the moving-grid code is not restricted to reaction-diffusion equations of type (1.1). The interested reader is referred to [2] and [33], where PDEs from various other application areas have been solved using this technique.

The boundary conditions are of Dirichlet type:

$$U(\tilde{x} = 0, t) = U(\tilde{x} = 1, t) = 1 \qquad V(\tilde{x} = 0, t) = V(\tilde{x} = 1, t) = 0.$$

Neumann conditions were also used, but did not influence the inner solutions. Moreover, the initial data for the results we report consists of a sharp pulse centred in the middle of the spatial domain: $U(\tilde{x}, 0) = 1 - \frac{1}{2}\sin^{100}(\pi\tilde{x})$, and $V(\tilde{x}, t = 0) = \frac{1}{4}\sin(\pi\tilde{x})$. The spatial

variable $\tilde{x}$ is a rescaled version of the spatial variable x in (1.1): $\tilde{x}$ has been scaled such that the numerical simulations always take place on the $\tilde{x}$-interval $[0, 1]$.

Since we wanted to be able to observe patterns described by the analysis of this paper, we focused in the numerical simulations on values of a and b which are $\mathcal{O}(1)$ with respect to δ. Our search in the (a, b)-parameter space of (1.1) has not yet found patterns that differ essentially from the ones described and shown below (by contrast, for larger a, we have observed various different patterns; an example is shown in section 7, figure 10, of a structurally different pattern at $a = 9$, $b = 0.4$ and $\delta^2 = 0.01$). Moreover, especially the dynamic splittings—the self-replications of the travelling pulses—are driven by processes which are very sensitive to the numerical accuracy: if there are not enough grid points 'on' a V-pulse, a splitting just cannot occur, or occurs much later. Thus, if one does not use enough grid points (or a non-moving grid) one is tempted to conclude that the self-replicating process does not occur. This observation also means that the error made by the code can 'explode' in a very short amount of time. For all numerical tests we have used 400 moving grid points to take care of the sharp pulses. In one case (20 pulses, $t_{\text{end}} = 20\,000$) 600 grid points had to be used (figures 7 and 8). Note that a conventional non-moving uniform would have required several (4–5) times more grid points than used for the moving-grid case.

Moreover, we found that decreasing δ increased both the (temporal) distance between successive splittings and the number of necessary grid points so drastically that one approaches very rapidly the limits of the machine one is working on for $\delta^2 \ll 0.01$ if one is interested in the long-time behaviour of the self-replicating patterns (see section 6.3 and figures 7 and 8).

Before we start the description of the patterns observed in the numerical simulations we remark on the magnitude of δ, both as a small quantity in our asymptotic analysis and as part of the data in the numerical simulations. First we note that by our scalings $\varepsilon = \delta^{1/3}$ (see (2.8), $\alpha = 1$) is the 'true' asymptotically small quantity of the analysis. This means that a 'standard' choice of $\varepsilon = 0.1$ corresponds to a value of $\delta^2 = 10^{-6}$ as input in the numerical simulations of equation (1.1). On the other hand we noted that choices of $\delta^2 = 0.003$ are already near the boundary of the capacity of the hardware and software one is using. Thus, theoretically, one expects only a small overlap between the numerically 'safe' and the analytically 'safe' regions. However, we shall see that there is a good qualitative and quantitative agreement between the analytical predictions and the numerical observations.

6.2. Stationary behaviour and a transition region

In the bifurcation analysis we performed, we fixed b at a certain value, $b \in (0.2, 1)$, and varied a over a certain range, $a \in (0.2, 5)$ (approximately). For each parameter pair, we repeated the simulations for several values of δ, but we found that the value of δ did not have an essential influence on the dynamics, except for the time scale of the evolution. For $a > 0$ 'too small', we observed the following behaviour:

$$\lim_{t\to\infty} U(x, t) \equiv 1 \qquad \lim_{t\to\infty} V(x, t) \equiv 0.$$

Note that this is not completely surprising, since the trivial pattern ($U \equiv 1, V \equiv 0$) is an asymptotically stable solution of (1.1) on the unbounded domain.

As we increase a, we enter a transition region between the trivial behaviour and the self-replicating pulse regime. Moreover, we find that the transition region is not a clear one-dimensional bifurcation curve in the (a, b)-parameter space, and the behaviour in the transition region depends rather subtly on the initial conditions and small perturbations.

First, we observe stable, stationary solitary-pulse solutions of the type constructed in section 4.1 (see figure 1 in section 2). These solutions of (1.1) are precisely the one-circuit slow/fast homoclinic described by theorem 4.1, and they seem to be stable in this transition region (see below for a quantitative check). In figure 1, we show plots of $U(x,t)$ and $V(x,t)$ for $a = 1$ and $b = 0.6$. Note that they are insensitive to the details of the initial one-pulse concentration.

Second, we find parameter values at which initial solitary pulses split into two non-travelling pulses. These depend sensitively on the initial concentrations in the interval. These patterns do *not* correspond to the two-circuit homoclinic solutions described by theorem 4.1 ($N = 2$): V becomes exponentially small between the two fast excursions, while the two-circuit pulse described by theorem 4.1 does not approach the slow manifold $\mathcal{M}$ closer than $\mathcal{O}(\sqrt{\varepsilon})$ during its circuits through the fast field. Using the symmetry (4.1) it is not hard to show that such a solution to the stationary problem (1.4) or (2.9) with $\gamma = 0$ does not exist: a homoclinic solution which takes off at $\ell^U \cap T_o$ can only touch down exactly on $\ell^S \cap T_d$. This is confirmed by the numerics: although the pulses do not move, the two-pulse pattern is not stationary. In figure 5, we see that the heights of the two pulses 'dance' up and down until one of them disappears completely and only a stationary solitary pulse remains. Note that this pulse is not located exactly in the middle of the x-interval, contrary to the initial values of U and V. We found that the length and the outcome of this process (i.e. the answer to the question: 'which pulse disappears after what period of time?') depends very sensitively on small perturbations. It also depends on the width of the initial V-pulse whether the solutions V undergoes an initial splitting, as in figure 5, or whether it does not. In the latter case, the initial solution deforms immediately into a stationary solitary peak described by theorem 1 ($N = 1$) (see figure 1(a): the pulse is exactly at the middle of the x-interval).

We now compare the outcome of the numerical simulations with the analytical results of section 4.1. We show numerically stable stationary one-pulses for $a = 1$, $b = 0.6$, with $\delta^2 = 0.01$ in figure 1(a) and with $\delta^2 = 0.003$ in figure 1(b). Numerically, we find:

$$\delta^2 = 0.01: \qquad V_{\max} \approx 1.11 \qquad U_{\min} \approx 0.16$$
$$\delta^2 = 0.003: \qquad V_{\max} \approx 1.49 \qquad U_{\min} \approx 0.08.$$

Since $B = b\delta^{2/3}$, (4.13) implies:

$$\delta^2 = 0.01: \qquad V_{\max} \approx 1.39 \qquad U_{\min} \approx 0.14$$
$$\delta^2 = 0.003: \qquad V_{\max} \approx 1.69 \qquad U_{\min} \approx 0.076$$

to leading order. The leading-order correction to $\hat{v}_{\max}$, the $\mathcal{O}(1)$ scaled version of $V_{\max}$, is $\mathcal{O}(\varepsilon)$. By (2.4) we see that $V_{\max}$ is $\mathcal{O}(\frac{1}{\varepsilon})$ to leading order, with $\varepsilon = \delta^{1/3}$ ((2.8) and $\alpha = 1$). We conclude that the leading-order correction in the above-determined theoretical value of $V_{\max}$ is $\mathcal{O}(1)$. The differences between the numerically observed values of $V_{\max}$ and the theoretical predictions are clearly within this range. Furthermore, we note that the relative error, $|V_{\max}^{\text{num}} - V_{\max}^{\text{theo}}|/V_{\max}^{\text{num}}$, decreases as δ is decreased (from ≈ 0.25 for $\delta^2 = 0.01$ to ≈ 0.13 for $\delta^2 = 0.003$) and that these errors are again well within the theoretical bound of $\mathcal{O}(\varepsilon)$ ($\varepsilon \approx 0.46$ for $\delta^2 = 0.01$ and $\varepsilon \approx 0.38$ for $\delta^2 = 0.003$). A similar argument yields that the distance between the numerically observed value of $U_{\min}$ and the above theoretical prediction is within the leading order correction to the theoretical value of $U_{\min}$ of $\mathcal{O}(\varepsilon\delta) = \mathcal{O}(\varepsilon^4)$ ($\varepsilon^4 \approx 0.046$ for $\delta^2 = 0.01$, $\varepsilon^4 \approx 0.021$ for $\delta^2 = 0.003$).

One might expect that it should be possible to find a (numerically stable) two-circuit pulse solution—as described by theorem 4.1 for $N = 2$—in this transition region, by varying the initial conditions. We did not do an extensive numerical search to find these solutions;

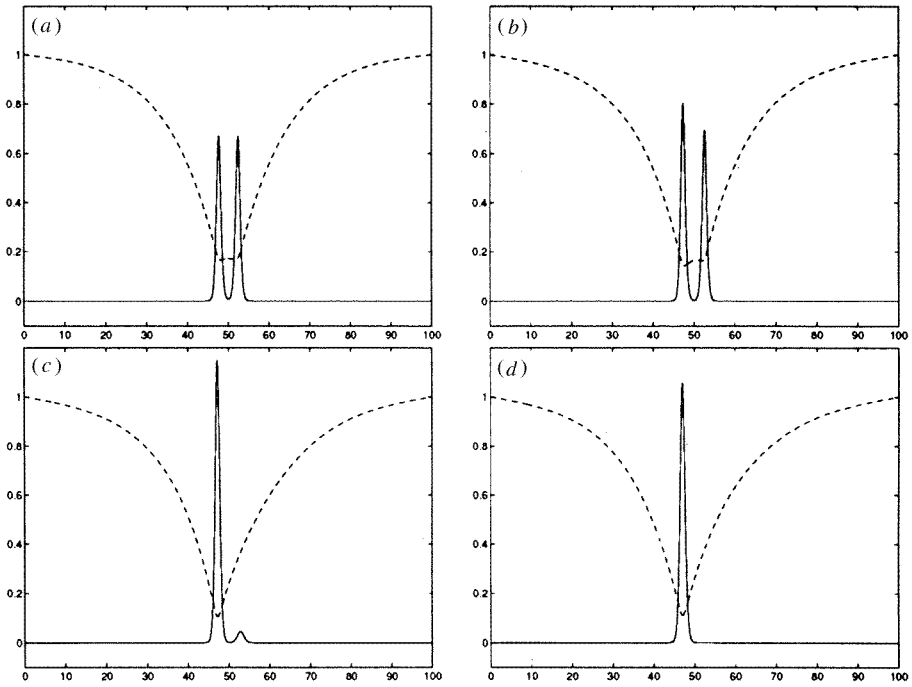

Figure 5. A pair of dancing pulses observed in numerical simulations of (1.1) with $a = 0.6$, $b = 0.4$, and $\delta^2 = 0.01$: (a) at time $t = 250$; (b) at time $t = 350$; (c) at time $t = 450$; and (d) at time $t = 500$, showing that only the left pulse survives as a stable solitary pulse in the asymptotic state. The concentration, U, is given by a broken curve, and the concentration, V, is denoted by a full curve.

however, we did find that in the transition from initial data which splits into two solitary 'dancing' pulses to a non-splitting initial condition, there exist initial conditions that initiate solutions which are like the stationary two-circuit pulse for a very long time (but, eventually, V becomes exponentially small between the peaks and the 'dancing behaviour' starts).

6.3. Self-replicating pulses

For values of a above this transition region (with b still fixed), we observe that the two solitary pulses created from the initial condition at the first, stationary splitting begin to move away from each other, both with the same, constant speed (see below for a discussion on the magnitude of this speed). We know from section 5 that these patterns cannot be interpreted as some kind of nonlinear superposition of two solitary travelling pulses with speeds c and $-c$: these solutions do not exist. This observation is remarkable, if one only pays attention to the V solution, since V seems to be exponentially small between the two travelling peaks (see figure 6(a), where $a = 2$). However, U does not 'return' to 1 in between the pulses, which should be the case for the solitary travelling waves studied in section 5. On the other hand, the maximum value of U between the two travelling V-pulses grows towards 1 as the distance between these pulses grows: the travelling pulses begin to resemble the non-existing solitary pulses more and more. A conflict with the non-existence result of theorem 5.1 would occur if these pulses go on travelling away from each other with constant speed, without changing shape, while the value of U approaches 1 'in the

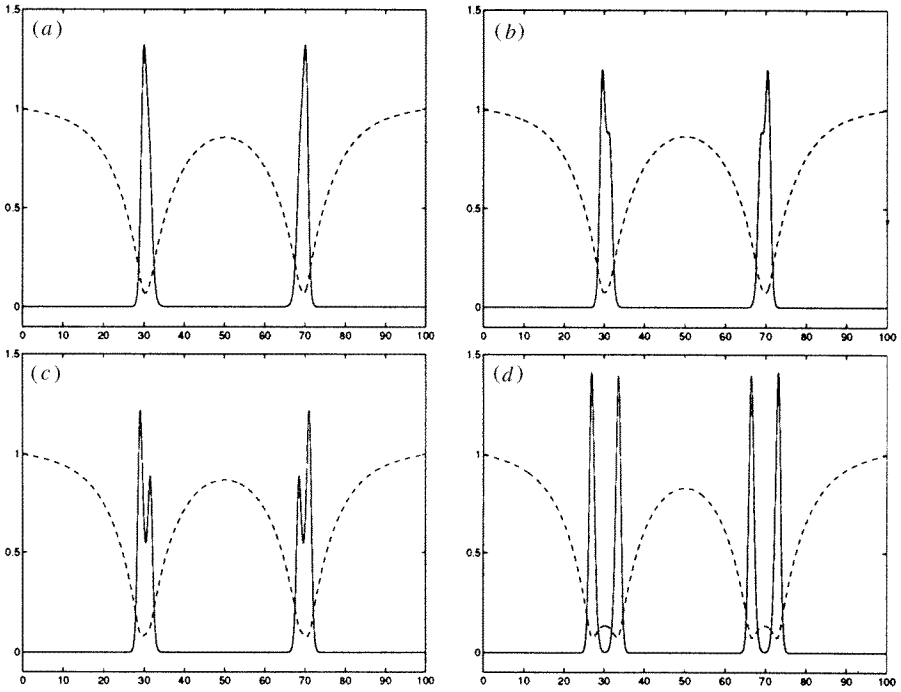

Figure 6. The dynamic pulse-splitting process at times: (*a*) $t = 2100$; (*b*) $t = 2150$; (*c*) $t = 2200$; and (*d*) $t = 2400$. New pulses are formed on the trailing (inner) edges of the existing two pulses (near the x-values corresponding to the inflection points of U) and are sent into the centre of the domain. Here $a = 2$, $b = 0.4$, and $\delta^2 = 0.01$.

middle': both pulses then become identical to the solitary travelling pulses considered in section 5.

Therefore, something else must happen: for $a = 2$, we see in figures 6(*b*)–(*d*) that both V pulses split into two similar travelling pulses (with distinct speed) yielding a pattern of four moving pulses. After yet more time, all four of these V pulses split once again, and this process of replication continues for the outermost two pulses on each side until an equilibrium state is reached. In fact, the number of peaks a domain can support depends on a and b. In figure 7, we show the solutions U and V at time $t = 20\,000$ for the choice of parameters $a = 2$, $b = 0.4$ and $\delta^2 = 0.01$. There are 20 peaks present.

For the same simulation shown in figure 7, we plot the positions of the grid points of our code as functions of time in figure 8. The position of the V pulses is revealed by a local concentration of grid points. Thus, due to the character of the code, we can follow the pulses and their self-replicating behaviour by plotting the positions of the grid points. Note that the horizontal bands in figure 8 just indicate the fact that one (or more) of the pulses 'needs more grid points' since it is near a self-replication: the other pulses 'send' some of 'their' grid points to the self-replicating one(s). Thus, the horizontal bands suggest dynamical behaviour for a large x-interval, but, the dynamics are only local, near a number of self-replicating pulses, for the solutions (U, V) of the PDE (1.1).

From these observations, as well as from those of many other initial data, it seems *a priori* that the solutions to (1.1) with A (*a*) and B (*b*) in the splitting region have a strictly non-stationary behaviour. However, we observe in figure 8 that only the outermost pairs of

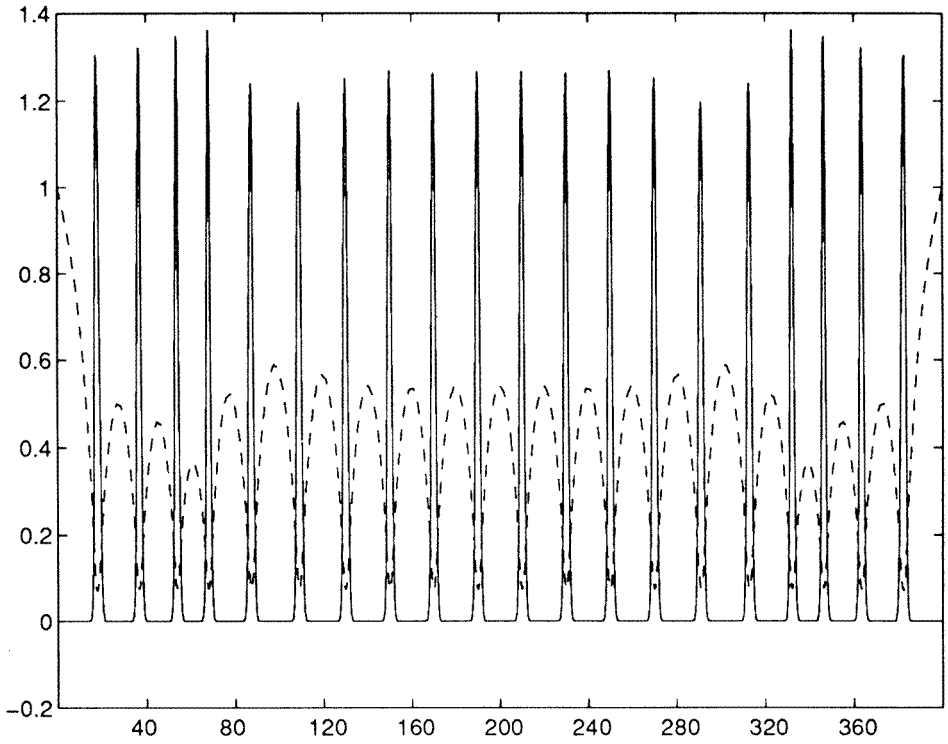

Figure 7. The pulse pattern observed at $t = 20\,000$ for $a = 2$, $b = 0.4$, and $\delta^2 = 0.01$, where 600 moving grid points were used.

pulses continue the self-replicating process: after a pulse has been created by a 'boundary pulse' it only splits just one more time. The two resulting pulses are then enclosed by other pulses: it is as if the pulses are repelling each other. As a consequence, we observe that the core of the pattern created by the self-replicating process is a *stationary, periodic pattern of the type described by theorem 4.2*: it clearly has distinguished slow and fast parts. This can also be seen in figure 7: the pattern in the middle (middle 6 peaks) is clearly periodic in U and V. It follows from grid dynamics (figure 8) that this periodic core is also stationary. Note also that the splittings of the boundary pulses and their latest images have a tendency to occur simultaneously after sufficiently large times in this simulation. Lastly, we remark that in addition to this outer pair splitting process, we have observed other sequences of pulse splittings. However, after 'long' times, all of these patterns had periodic cores described by the stationary periodic solutions of theorem 4.2. Moreover, the $U_{\max}$ and $\mathcal{T}_P$ of these cores were accurately related by the theoretically deduced equations (4.10) and (4.11).

This statement is also readily verified quantitatively in the simulations. We make a quantitative comparison of the periodic core properties of the pattern in figure 7 with the periodic solutions constructed in section 4.2. Numerically, for the case shown in figure 7, we find that:

$$\mathcal{T}_P \approx 20 \qquad U_{\max} \approx 0.54 \qquad V_{\max} \approx 1.26 \qquad U_{\min} \approx 0.07.$$

We know from section 4.2 that $\mathcal{T}_P$ and $U_{\max}$ are related by (4.10) or (4.11). Inserting $U_{\max} = 0.54$ into (4.10) gives $\mathcal{T}_P \approx 19.97$ (where $a = 2$, $b = 0.4$ and $\delta^2 = 0.01$). Equivalently, we find that inserting $\mathcal{T} = 20$ into (4.11) yields a value of $U_{\max}$ which agrees

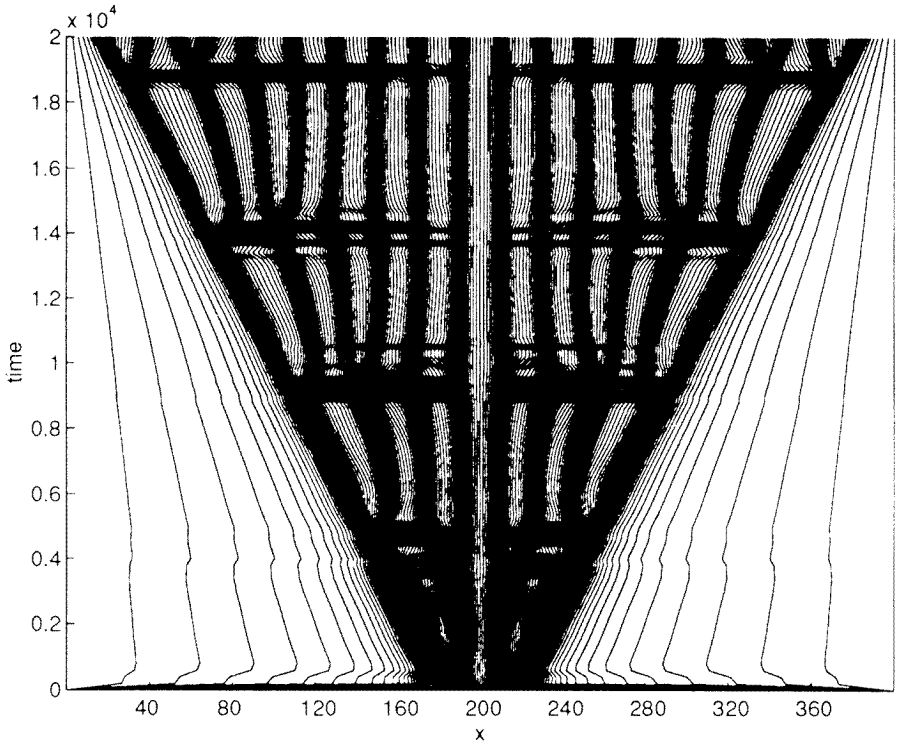

Figure 8. Positions of the grid points as functions of time for the moving grid code described in section 6.1 for the same parameters as used in figure 7. Note that the first dynamic splitting occurs earlier than in figure 6 (although $a = 2$, $b = 0.4$ and $\delta^2 = 0.01$ in both cases): the simulations have different initial conditions (the initial conditions are the same in the rescaled variable $\tilde{x}$).

with the numerically observed one. The fact that the numerically measured values of $\mathcal{T}_P$ and $U_{\max}$ obey the relations (4.10) and (4.11) with this accuracy is a bit surprising: both (4.10) and (4.11) are just the leading-order approximations. Nevertheless, this result at least indicates that the stationary periodic patterns at the core of the self-replicating patterns are described by the slow/fast periodic solutions of theorem 4.2. Moreover, we can use (4.12) to 'predict' the leading-order values of $V_{\max}$ and $U_{\min}$ for this pattern: $V_{\max} \approx 2.14$ and $U_{\min} \approx 0.06$. Both values differ from the numerically observed values by an amount which is of the order of the leading-order corrections to (4.12) determined above.

Finally, we remark on the speed $\pm c$ of the 'boundary pulses' of the self-replicating pattern. It is clear from figure 8 that this speed is (at least at leading order) constant for all time. We noted that this speed approaches zero as a decreases towards the above described transition region. Thus, c clearly depends on a and b. However, c also depends on δ. We have seen in section 5 that the magnitude of c with respect to δ does have an essential influence on the singular perturbation analysis. Therefore, we performed the following experiment: we fixed $a = 2$ and $b = 0.4$, and we varied δ^2. We waited until the 'boundary pulses' were created and moved, and then we measured their speed c. In figure 9, we present a log–log plot of this c as a function of δ: c is clearly $\mathcal{O}(\delta^2)$. Note that this is exactly the value at which significant degeneration of the asymptotic analysis occurs, as encountered in section 5.

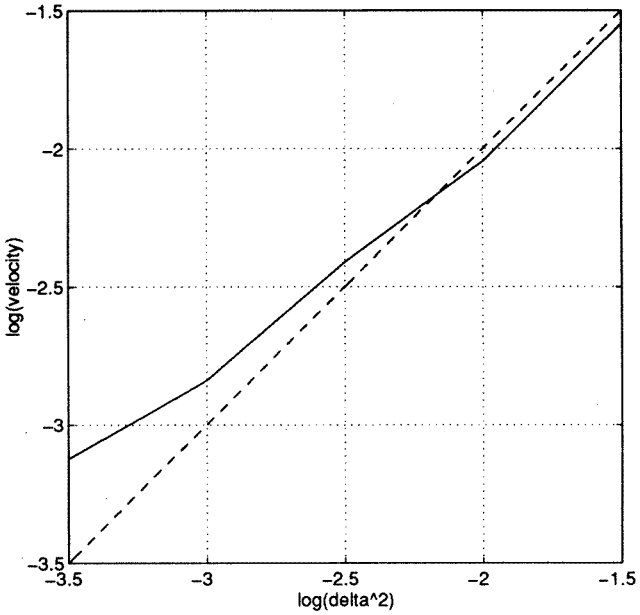

Figure 9. The log–log plot of the speed with which the outermost pulses travel as a function of δ showing that this speed scales as $\mathcal{O}(\delta^2)$; a and b are kept fixed at $a = 2$, $b = 0.4$.

7. Discussion

We have proven the existence of single-pulse solutions for any a and b (the rescaled versions (2.4) of A and B in (1.1)). However, only those with a and b in the transition region described in section 6 are observed, and thus probably stable. A similar selection occurs for the periodic patterns constructed in section 4.2: for any a, b and $U_{\max} < 1$ ($U_{\max} = \mathcal{O}(1)$) there exists a stationary periodic pulse pattern, but periodic patterns are only observed for parameter values (a, b) in the self-replicating pulse region (section 6). Moreover, $U_{\max}$ is also selected by the process. Furthermore, the numerical simulations suggest that also the parameter α, which we can choose in the interval $[0, \frac{3}{2})$ in the analysis of section 4, is the subject of a selection process: our simulations and those in [22] suggest that $\alpha \approx 1$ (note that α is determined by the magnitude of B with respect to δ (remark 2.4), therefore, it is not possible to determine α exactly, for given values of δ and B). Determining the analytical origin of these selection mechanisms is the subject of future research.

In addition, the pulse-splitting process requires considerable further analysis. A chemical explanation has been given for when the dynamic splitting should commence—indicating that the onset time coincides with the time at which the flux of $\mathcal{U}$ into the tail of the moving pulse exceeds the minimum level needed to sustain a new pulse [22]. A formal mathematical analysis for pulse-splitting has been developed in [22, 23]. Our simulations suggest that the process occurs largely at the 'fronts' of the moving-pulse pattern. In particular, for the simulation reported in section 6.3, the outermost pair of moving pulses on each side were the ones that self replicated, and as time progressed, these self-replicating edge pairs created the stationary, periodic core of the self-replicating pulse pattern. This observation is consistent with the chemistry explanation in the sense that only between the new, outermost, pulses is there enough $\mathcal{U}$ present (both from the as yet unconsumed supply

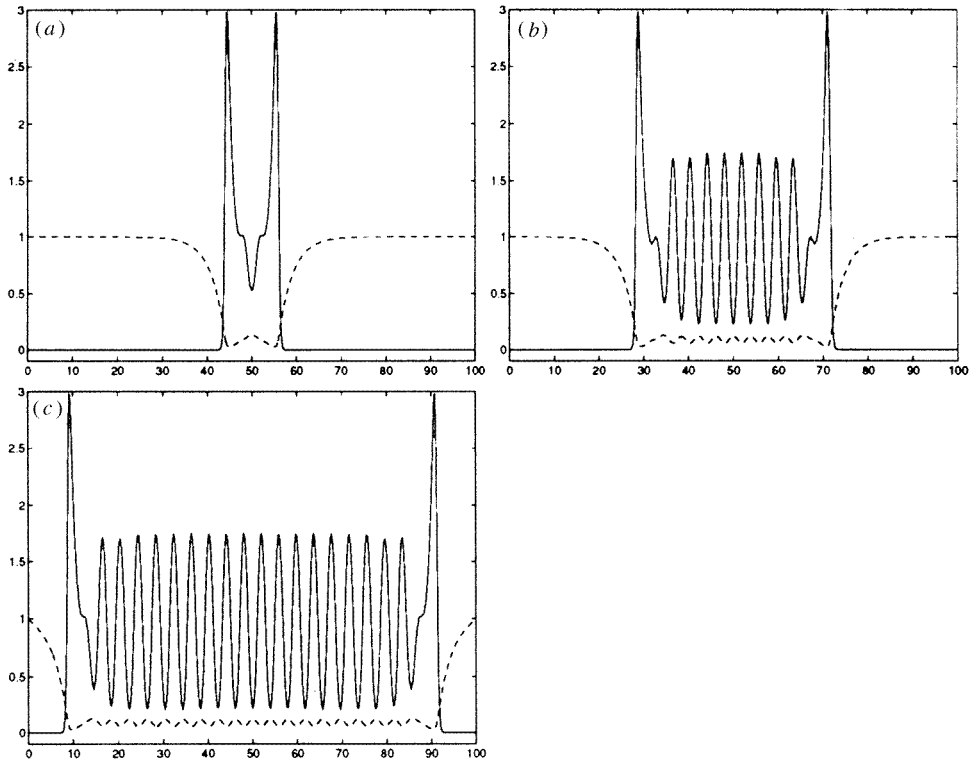

Figure 10. A plot of the solution to (1.1) with parameter $a \neq \mathcal{O}(1)$: $a = 9$, $b = 0.4$, $\delta^2 = 0.01$: (*a*) at $t = 100$, (*b*) at $t = 500$, and (*c*) at $t = 1000$. As in figure 7 there is a stationary periodic core, but it has not been created by a pulse-splitting process.

available in the domain and from the reservoir) to create new pulses. By contrast, in the core region, all of the $\mathcal{U}$ supplied by the reservoir is needed to maintain the already existing pulses, and there is very little excess (free, unconsumed) $\mathcal{U}$ in between the pulses.

Although we did not perform any detailed analysis on the system with $A > \mathcal{O}(\delta^2)$, we believe that an approach similar to that established here—based on a different scaling of the parameters and variables—can be used in this region of phase space. The combination of such an analysis and simulations might give another explanation of the origin of the self-replicating pulse process. In figure 10, we plot the results of a simulation with $a = 9$, $b = 0.4$ and $\delta^2 = 0.01$. Thus, it is not natural to assume that $A = a\delta^2 = \mathcal{O}(\delta^2)$. However, just as in the case $a = \mathcal{O}(1)$ a first stationary splitting occurs, but, V does not become exponentially small between the two travelling boundary pulses (figure 10(*a*)). Moreover, we observe that U remains small in that region: it seems that the slow manifold $\mathcal{M}$ is much less important in this case. No pulse-splitting occurs, but, after some time there is again a stationary periodic core (see figure 10(*b*) and (*c*)). This core is now formed by a stationary solution which 'lives' entirely in the fast field. As we decrease a we observe that the pulse-splitting process starts as soon as the periodic orbit at the core of the pattern touches down on $\mathcal{M}$. For completeness we note that the choice of parameters for the simulation of figure 10 is a little bit outside the chemical relevant region since $A = a\delta^2 = 0.09 > B = b\delta^{2/3} \approx 0.086$ (see remark 2.3). However, the pattern does not change significantly if we decrease a a little such that $A < B$.

Note that it is not hard to show that the 'purely fast' stationary periodic orbits do not exist in our scaled system (2.5) and (2.9): the accumulated change in p along such an orbit cannot be zero (cf (3.18)). However, such orbits can be created by a Hopf bifurcation around critical points in the fast field of the unscaled (1.4) system which exist if $A > 4B^2$ (see also [11, 22]). These critical points did not appear in this paper since A cannot be larger than $4B^2$ by the scalings ((2.4), $\alpha < \frac{3}{2}$) derived in this paper. Analogously, one can say that the fact that the pulse patterns are not observed for values of A and B outside the region defined by our scalings, justifies these scalings: they were derived as necessary conditions for the existence of the pulse-like solutions (see section 2). Thus, the phenomena described above cannot be described by the main equations of this paper, (2.5) and (2.9), but we believe that they can be studied by methods similar to those employed in this paper.

It is clear that all of the necessary ingredients of the analysis in this paper also exist in other systems of the general form:

$$\begin{aligned} \frac{\partial U}{\partial t} &= \nabla^2 U + f_1(U, V) \\ \frac{\partial V}{\partial t} &= \delta^2 \nabla^2 V + f_2(U, V) \end{aligned} \tag{7.1}$$

where f_1 and f_2 satisfy some additional conditions. In particular, the nonlinearities must be such that the fast kinetics have one or more equilibria connected to themselves by homoclinic or heteroclinic orbits. In addition, the slow subsystems must possess either equilibria with stable and unstable manifolds or other orbit segments that are transverse to the appropriate take-off and touch-down curves defined by the fast homoclinics and/or heteroclinics. Once again one can check numerically whether the constructed patterns can be stable. Moreover, whether the non-existence of travelling waves plays a role in signalling that a general system exhibits pulse replication can also be investigated, since *a priori* it is not clear that general systems of the form (7.1) which do have (stable) stationary pulse-like patterns share the nonexistence result of (1.1).

Acknowledgments

The authors thank Thomas Erneux for suggesting this subject to them. We also thank Wiktor Eckhaus for his very useful suggestions and for helping us pinpoint an error in the initial formulation. This research was partially supported and financed by the Netherlands Organization for Scientific Research (NWO). TK thanks the Mathematisch Instituut of the Universiteit Utrecht for its hospitality during the Summer of 1995. TK also gratefully acknowledges partial funding from the National Science Foundation through grant DMS-9307074 and from the Alfred P Sloan Foundation in the form of a Sloan Research Fellowship.

Appendix. Details of the scaling analysis

In this appendix, we derive the scalings (2.4) presented in section 2. We begin by plugging in the rescaled u and γ (2.3) into the fast field, which is the fast (v, q) part of (1.4):

$$\begin{aligned} \dot{v} &\equiv v_\eta = q \\ \dot{q} &\equiv q_\eta = -\delta^\beta \hat{\gamma} q - \delta^\alpha \hat{u} v^2 + Bv. \end{aligned} \tag{A.1}$$

The fast system (A.1) is linear in the limit $\delta \to 0$ (if $\alpha > 0$) and has no solutions which are homoclinic to the saddle point $(v, q) = (0, 0)$. This is a crucial deficiency of the fast field, since this—again—means that a solution which leaves the neighbourhood of $\mathcal{M}$ cannot return to $\mathcal{M}$. Thus, in order to be able to construct homoclinic solutions to S, we need scalings of v, q and B such that the leading-order fast field supports homoclinic solutions. In particular, we introduce $v = \delta^{-r}\hat{v}$, $r > 0$ and $q = \delta^{s}\hat{q}$; here r and s are free parameters which will be determined later on. We balance the $\hat{u}v^2$ and Bv terms in (A.1) by setting $B = \delta^{(\alpha-r)}b$. We now observe that $\hat{v}_\eta = \mathcal{O}(\delta^{(r+s)})$ and $\hat{q}_\eta = \mathcal{O}(\delta^{(\alpha-2r-s)})$. We impose $r+s = \alpha-2r-s$, since the distinguished limit in the second-order $\hat{v}$ equation occurs when $\hat{v}$ and its derivative $\hat{q}$ evolve on the same time scale. Thus, $s = \frac{1}{2}(\alpha - 3r)$. Introducing the new independent variable $\hat{\eta} = \delta^{\frac{1}{2}(\alpha-r)}\eta$, (A.1) transforms to:

$$\begin{aligned} \hat{v}_{\hat{\eta}} &= \hat{q} \\ \hat{q}_{\hat{\eta}} &= -\hat{u}\hat{v}^2 + b\hat{v} - \delta^{\frac{1}{2}(2\beta-\alpha+r)}\hat{\gamma}\hat{q}. \end{aligned} \tag{A.2}$$

This equation has all necessary features so that it can serve as fast field in the rescaled version of (1.4). Note that we again have to impose that the 'friction' term $\hat{\gamma}\hat{q}$ is o(1), i.e. $2\beta - \alpha + r > 0$.

When we introduce all the above scalings, supplemented with a scaling for p: $p = \delta^t\hat{p}$ for some $t > 0$, into the slow part of (1.4), we find that $\hat{u}_{\hat{\eta}} = \mathcal{O}(\delta^{\frac{1}{2}(r+2t+2-3\alpha)})$ and $\hat{p}_{\hat{\eta}} = \mathcal{O}(\delta^{\frac{1}{2}(2+\alpha-3r-2t)})$ (i.e. the '$\hat{u}\hat{v}^2$'-term is the leading order term in $\hat{p}_{\hat{\eta}}$, the other terms in $\hat{p}_{\hat{\eta}}$ are assumed to be o(1)). Since the distinguished limit also occurs when the dependent variable—here $\hat{u}$—varies at the same rate as its derivative, we set $t = \alpha - r$. This gives the following rescaled equations:

$$\begin{aligned} \hat{u}_{\hat{\eta}} &= \delta^{\frac{1}{2}(2-\alpha-r)}\hat{p} \\ \hat{p}_{\hat{\eta}} &= \delta^{\frac{1}{2}(2-\alpha-r)}[\hat{u}\hat{v}^2 - \delta^{(1+\beta+r)}\hat{\gamma}\hat{p} - \delta^{(2+2r-\alpha)}a + \delta^{2+2r}a\hat{u}] \end{aligned} \tag{A.3}$$

with the additional assumption $2 - \alpha - r > 0$, so that the $(\hat{u}, \hat{p})$-subsystem remains slow compared to the $(\hat{v}, \hat{q})$-subsystem.

Combining the fast and the slow subsystems (A.2) and (A.3), we note that there are two different leading-order perturbation scales: the slow 'time'-scale $\delta^{\frac{1}{2}(2-\alpha-r)}$ in (A.3) and the 'friction'-term of $\mathcal{O}(\delta^{\frac{1}{2}(2\beta-\alpha+r)})$ in (A.2). It follows from the analysis presented in section 3 that the stable and unstable manifolds of the slow manifold $\mathcal{M}$ can only intersect if the friction-term is of the same order as the square of the leading-order term $\delta^{\frac{1}{2}(2-\alpha-r)}$ in (A.3) (i.e. it is of $\mathcal{O}(\delta^{(2-\alpha-r)})$) for the existence of the desired homoclinic solution $\Gamma_h(\eta)$. Thus, a homoclinic solution $\Gamma_h(\eta)$ to $S \in \mathcal{M}$ can only exist if the leading-order perturbation in the complete $(\hat{u}, \hat{p}, \hat{v}, \hat{q})$-system is $\mathcal{O}(\delta^{\frac{1}{2}(2-\alpha-r)})$. Hence, when a solution makes an excursion through the fast field, one expects that both $\hat{u}$ and $\hat{p}$ will change by an amount of $\mathcal{O}(\delta^{\frac{1}{2}(2-\alpha-r)})$. Since $p = \delta^{(\alpha-r)}\hat{p}$, this implies that an excursion through the fast field modifies p by an amount of $\mathcal{O}(\delta^{\frac{1}{2}(2+\alpha-3r)})$. The homoclinic solution $\Gamma_h(\eta)$ must 'jump' from ℓ^U to ℓ^S (2.2) by such an excursion through the fast field. Due to the scaling (2.1), we know that ℓ^U and ℓ^S are $\mathcal{O}(\delta)$ apart; thus, we have to choose r such that it satisfies the following 'jump condition': $\frac{1}{2}(2 + \alpha - 3r) = 1 \quad \text{or} \quad r = \frac{1}{3}\alpha$. With this value of r, one directly obtains the scalings given in (2.4).

References

[1] Becker P K and Field R J 1985 Stationary concentration patterns in the oregonator model of the Belousov–Zhabotinski reaction, *J. Phys. Chem.* **89** 118–28

[2] Blom J G and Zegeling P A 1994 Algorithm 731: a moving-grid interface for systems of one-dimensional time-dependent partial differential equations *ACM Trans. Math. Software* **20** 194–214

[3] Dawson S P, Hasslacher B and Pearson J E 1996 Lattice gas simulations of replicating domains, *Pattern Formation and Lattice Gas Automata (Proc. NATO Workshop, Waterloo, Canada, June 1993) (Fields Institute Communications)* ed A Lawniczak and R Kapral (Providence, RI: American Mathematical Society)

[4] Dewel G and Borckmans P 1990 Localized structures in reaction-diffusion systems *Patterns, Defects, and Material Instabilities* ed D Walgraef and N M Ghoniem (Dordrecht: Kluwer) pp 63–72

[5] Eckhaus W 1979 *Asymptotic Analysis of Singular Perturbations* (Amsterdam: North-Holland)

[6] Ermentrout G B, Hastings S P and Troy W C 1984 Large amplitude stationary waves in an excitable lateral-inhibitory medium *SIAM J. Math. Anal.* **44** 1133–49

[7] Fenichel N 1979 Geometrical singular perturbation theory for ordinary differential equations *J. Diff. Eqns* **31** 53–98

[8] Goldstein R E, Muraki D J and Petrich D M 1996 Interface proliferation and the growth of labyrinths in a reaction-diffusion system *Phys. Rev.* E **53** 3933–57

[9] Gray P and Scott S K 1983 Autocatalytic reactions in the isothermal, continuous stirred tank reactor: isolas and other forms of multistability *Chem. Eng. Sci.* **38** 29–43

[10] Gray P and Scott S K 1984 Autocatalytic reactions in the isothermal, continuous stirred tank reactor: oscillations and instabilities in the system $A + 2B \rightarrow 3B$, $B \rightarrow C$ *Chem. Eng. Sci.* **39** 1087–97

[11] Gray P and Scott S K 1985 Sustained oscillations and other exotic patterns of behaviour in isothermal reactions *J. Phys. Chem.* **89** 22–32

[12] Jones C K R T 1995 Geometric singular perturbation theory, *Dynamical Systems (Montecatibi Terme, 1994) (Lecture Notes in Mathematics 1609)* ed R Johnson (Berlin: Springer)

[13] Jones C K R T, Kaper T J and Kopell N 1996 Tracking invariant manifolds up to exponentially small errors *SIAM J. Math. Anal.* **27** 558–77

[14] Kapral R 1995 Pattern formation in chemical systems *Physica* **86D** 149–57

[15] Landau L D and Lifschitz E M 1977 Quantum mechanics: non-relativistic theory *Course on Theoretical Physics* vol 3, 3rd edn (Oxford: Pergamon)

[16] Lee K J, McCormick W D, Ouyang Q and Swinney H L 1993 Pattern formation by interacting chemical fronts *Science* **261** 192–4

[17] Lin K-J, McCormick W D, Pearson J E and Swinney H L 1994 Experimental observation of self-replicating spots in a reaction-diffusion system *Nature* **369** 215–18

[18] Malevents A, Careta A and Kapral R 1995 Biscale chaos in propagating fronts *Phys. Rev.* E **52** 4724

[19] Palmer K 1986 Transversal heteroclinic points and Cherry's example of a nonintegrable Hamiltonian system *J. Diff. Eqns* **65** 321–60

[20] Pearson J E and Horsthemke W 1989 Turing instabilities with nearly equal diffusion coefficients *J. Phys. Chem.* **90** 1588–99

[21] Pearson J E 1993 Complex patterns in a simple system *Science* **261** 189–92

[22] Reynolds W N, Pearson J E and Ponce-Dawson S 1994 Dynamics of self-replicating patterns in reaction diffusion systems *Phys. Rev. Lett.* **72** 2797–800

[23] Reynolds W N, Pearson J E and Ponce-Dawson S 1996 Self-replicating spots, submitted

[24] Robinson C 1983 Sustained resonance for a nonlinear system with slowly-varying coefficients *SIAM J. Math. Anal.* **14** 847–60

[25] Rohricht B and Horsthemke W 1991 A bifurcation sequence to stationary spatial patterns in a nonuniform chemical model system with equal diffusion coefficients *J. Chem. Phys.* **94** 4421–6

[26] Rovinsky A B 1991 Diffusive instabilities and pattern formation in the Belousov-Zhabotinsky reaction *Nonlinear Wave Processes in Excitable Media* ed A V Holden, M Markus and H G Othmer (New York: Plenum) pp 191–200

[27] Soto-Trevino C and Kaper T J 1995 Periodic orbits in singularly-perturbed systems, *Nonlinear Dynamics and Pattern Formation in the Natural Environment (Pitman Research Notes in Mathematics 335)* ed A Doelman and A van Harten pp 295–314

[28] Soto-Trevino C and Kaper T J 1995 Higher-order Melnikov theory for adiabatic systems *J. Math. Phys.* **37** 6220–49

[29] Turing A M 1952 The chemical basis of morphogenesis *Phil. Trans. R. Soc.* B **237** 37–72

[30] Vastano J A, Pearson J E, Horsthemke W and Swinney H L 1987 Chemical pattern formation with equal diffusion coefficients *Phys. Lett.* **124A** 320–4
[31] Vastano J A, Pearson J E, Horsthemke W and Swinney H L 1988 Turing patterns in an open reactor *J. Chem. Phys.* **88** 6175–81
[32] Wiggins S 1988 *Global Bifurcations and Chaos* (New York: Springer)
[33] Zegeling P A, Verwer J G and v Eijkeren J C H 1992 Application of a moving-grid method to a class of 1d brine transport problems in porous media *Int. J. Numer. Meth. Fluids* **15** 175–91